Research Square

Preprints are preliminary reports that have not undergone peer review.
They should not be considered conclusive, used to inform clinical practice,
or referenced by the media as validated information.

Antiviral CD8⁺ T cells Engage a Neuroimmune Circuit to Drive Anorexia

Kairui Mao

maok@xmu.edu.cn

State Key Laboratory of Cellular Stress Biology, School of Life Sciences, Faculty of Medicine and Life Sciences, Xiamen University

Chaoze Li

State Key Laboratory of Cellular Stress Biology, School of Life Sciences, Faculty of Medicine and Life Sciences, Xiamen University

Siyuan You

[illegible]

Yingchao Shang

State Key Laboratory of Cellular Stress Biology, School of Life Sciences, Faculty of Medicine and Life Sciences, Xiamen University

Cuiyun Li

State Key Laboratory of Cellular Stress Biology, School of Life Sciences, Faculty of Medicine and Life Sciences, Xiamen University

Huiqing Liang

State Key Laboratory of Cellular Stress Biology, School of Life Sciences, Faculty of Medicine and Life Sciences, Xiamen University

Xuemei Luan

State Key Laboratory of Cellular Stress Biology, School of Life Sciences, Faculty of Medicine and Life Sciences, Xiamen University

Jiaqin Li

State Key Laboratory of Cellular Stress Biology, School of Life Sciences, Faculty of Medicine and Life Sciences, Xiamen University

Shuqin Li

State Key Laboratory of Cellular Stress Biology, School of Life Sciences, Faculty of Medicine and Life Sciences, Xiamen University

Yuyan Shi

University of Science and Technology of China

Fang Liu

State Key Laboratory of Cellular Stress Biology, School of Life Sciences, Faculty of Medicine and Life Sciences, Xiamen University

Wenbo Lin
State Key Laboratory of Cellular Stress Biology, School of Life Sciences, Faculty of Medicine and Life Sciences, Xiamen University
Cheng Zhan
National Key Laboratory of Immune Response and Immunotherapy, Department of Hematology, The First Affiliated Hospital of USTC, Division of Life Sciences and Medicine, University of Science and Techn
https://orcid.org/0000-0001-9397-0871
Nengming Xiao
Xiamen University https://orcid.org/0000-0001-5417-707X
Hongling Huang
Xiamen University https://orcid.org/0009-0003-2655-399X

Biological Sciences - Article

Keywords:

Posted Date: November 10th, 2026

DOI: https://doi.org/10.21203/rs.3.rs-11546596/v1

License: This work is licensed under a Creative Commons Attribution 4.0 International License.
Read Full License

Additional Declarations: There is **NO** Competing Interest.

Antiviral CD8$^+$ T cells Engage a Neuroimmune Circuit to Drive Anorexia

Chaoze Li[1#], Siyuan You[1#], Yingchao Shang[1#], Cuiyun Li[1], Huiqing Liang[1], Xuemei Luan[1], Jiaqin Li[1], Shuqin Li[1,2], Yuyan Shi[3], Fang Liu[1], Wenbo Lin[1], Cheng Zhan[3], Nengming Xiao[1*], Hongling Huang[1*], Kairui Mao[1,2,4,5*]

[1] State Key Laboratory of Cellular Stress Biology, School of Life Sciences, School of Advanced Interdisciplinary Biomedical Sciences, Faculty of Medicine and Life Sciences, Xiamen University, Xiamen, 361102, China

[2] Scientific Research and lnnovation Center, Women and Children's Hospital, School of Medicine, Xiamen University, Xiamen, 361003, China.

[3] National Key Laboratory of Immune Response and Immunotherapy, Department of Hematology, The First Affiliated Hospital of USTC, Division of Life Sciences and Medicine, University of Science and Technology of China, Hefei, 230001, China

[4] Xiang'an Hospital of Xiamen University, School of Medicine, Faculty of Medicine and Life Sciences, Xiamen University, Xiamen, 361104, China.

[5] Laboratory Animal Center, Faculty of Medicine and Life Sciences, Xiamen University, Xiamen, 361102, China.

*Correspondence: Nengming Xiao, nengming@xmu.edu.cn;
Hongling Huang, honglinghuang@xmu.edu.cn;
Kairui Mao, maok@xmu.edu.cn

# These authors contributed equally to this work.

Abstract

Infection-induced anorexia is a conserved sickness response that contributes to host defense and tolerance[1-3]. Although innate immune mediators are known to induce anorexia through neuro-immune communication[1,4], whether and how adaptive immunity engages neural circuits to regulate feeding remains poorly understood. Here, we identify a neuro-immune pathway linking antigen-specific antiviral CD8$^+$ T-cell responses to brainstem control of feeding during lymphocytic choriomeningitis virus (LCMV) infection. Antigen-specific CD8$^+$ T cells were required for late-phase anorexia and neuronal activation in the nucleus of the solitary tract (NTS), where Vglut2$^+$ excitatory neurons mediated feeding suppression. Mechanistically, CD8$^+$ T cell-intrinsic ST2-MyD88 signaling promoted cytotoxic effector function and peripheral sympathetic nerve injury, while vagal afferent signaling conveyed peripheral neural perturbations to the brainstem. Chemical sympathetic denervation was sufficient to trigger NTS activation and anorexia, whereas sympathetic denervation before infection or disruption of the CD8$^+$ T-cell effector program attenuated these responses. Together, our findings reveal that IL-33-ST2-MyD88 signaling programs antiviral CD8$^+$ T-cell effector function to engage a peripheral sympathetic-vagal-brainstem axis that suppresses feeding. This work uncovers a neuro-immune mechanism by which adaptive antiviral immunity extends beyond pathogen control to orchestrate infection-associated behavioral adaptation.

Introduction

Infection elicits a coordinated set of behavioral adaptations, collectively termed sickness behavior, including anorexia, reduced locomotion, fatigue, and altered social interactions[1,5,6]. These evolutionarily conserved responses, particularly anorexia, may help prioritize energy allocation toward host defense and facilitate pathogen clearance[2,3,7]. However, prolonged anorexia can exacerbate tissue catabolism, disrupt metabolic homeostasis, and impair recovery[8,9]. Thus, infection-associated anorexia represents an important component of the host response, but its benefits must be balanced against the physiological costs of sustained nutrient deprivation.

Inflammation-associated anorexia arises from communication between the peripheral immune and central nervous systems, through which immune-derived signals are transmitted to the brain via humoral and neural pathways[1,10]. Through the humoral route, circulating inflammatory mediators act at specialized brain interfaces, including circumventricular organs (CVOs), to influence feeding-regulatory circuits[11]. For example, inflammatory mediators induced by lipopolysaccharide (LPS), including interleukin-1β (IL-1β) and prostaglandin E_2 (PGE_2), contribute to appetite suppression through central inflammatory signaling[4]. Similarly, growth differentiation factor 15 (GDF15) activates GFRAL-expressing neurons in the area postrema (AP) and nucleus of the solitary tract (NTS), whereas IL-6 contributes to anorexia and weight loss in cancer-associated cachexia[12,13]. In parallel, vagal and other sensory afferents convey peripheral inflammatory and tissue-derived signals to the brain[14,15]. These inputs converge on brainstem and downstream feeding-regulatory circuits, including the lateral parabrachial nucleus and central amygdala, to coordinate changes in food intake and other sickness behaviors[12,16,17]. Although the mechanisms through which innate immune responses engage these pathways are increasingly understood, whether and how pathogen-specific adaptive immune responses access and modulate neural circuits to orchestrate infection-associated anorexia remains largely unknown. Understanding this interplay is essential for elucidating how distinct stages of the immune response shape behavioral adaptations during infection.

Cytotoxic $CD8^+$ T cells are central to antiviral defense, eliminating infected cells through inflammatory mediators and cytotoxic mechanisms[18]. During chronic lymphocytic choriomeningitis virus (LCMV) infection, antigen-specific $CD8^+$ T cells differentiate into heterogeneous populations, including TCF-1^+ progenitor-exhausted cells, CX3CR1^+ effector-like cells, and terminally exhausted populations[19-22]. These differentiation trajectories are shaped by antigen stimulation, costimulatory signals, inflammatory cytokines, and tissue-derived cues[23]. Type I interferons (IFN-Is) promote antiviral activation but can accelerate T-cell exhaustion under sustained stimulation, whereas IL-21 supports antiviral $CD8^+$ T-cell responses and CX3CR1^+ effector populations[24,25]. IL-33 signaling through ST2 can further modulate $CD8^+$ T-cell expansion, effector function, and progenitor-cell maintenance[26,27]. Previous studies have demonstrated that $CD8^+$ T cells contribute to anorexia and weight loss during LCMV infection, establishing a link between adaptive antiviral immunity and infection-associated behavioral changes[28,29]. However, whether specific upstream signals direct the differentiation of $CD8^+$ T-cell subsets with distinct capacities to engage neuro-immune circuits, and how these subsets drive anorexia during viral infection, remain poorly understood. Elucidating these mechanisms may reveal how adaptive antiviral immunity coordinates pathogen control with behavioral and physiological responses.

Results

Virus-specific CD8$^+$ T cells trigger late phase anorexia during LCMV infection

During infection, the brain senses peripheral innate immune signals, including IL-1β, TNF, IL-6 and PGE_2, through humoral and neural pathways to induce sickness behaviors that coordinate host defense and tolerance[1,30]. Although these mechanisms have established innate immunity as a major driver of infection-associated changes in brain function and behavior, whether and how adaptive immunity communicates with the nervous system to shape sickness behavior remains largely unknown. To investigate the interaction between adaptive immunity and the nervous system, we employed the lymphocytic choriomeningitis virus (LCMV) clone 13 infection model and first characterized the temporal dynamics of feeding behavior. Following infection, mice exhibited a biphasic, transient and reversible reduction in both food intake and body weight, with a modest decline during the first 2 days followed by a markedly more pronounced phase between days 6 and 8 (Fig. 1a and b). Changes in food intake closely correlated with changes in body weight (Fig. 1c), indicating that reduced caloric intake is a major contributor to the pronounced weight loss. Notably, the temporal dynamics of feeding behavior closely paralleled the evolution of the host immune response: the early phase of anorexia coincided with innate immune activation, whereas the more pronounced late phase emerged with the development of adaptive immunity. These observations suggested that infection-associated anorexia may be dynamically regulated by distinct stages of the immune response and prompted us to investigate whether adaptive immunity engages specific neural circuits to control feeding during viral infection.

To determine whether the late-phase suppression of feeding was dependent on adaptive antiviral T-cell responses, we first infected *Tcra*$^{-/-}$ mice, which lack conventional αβ T cells, with LCMV. Compared with wild-type mice, *Tcra*$^{-/-}$ animals were largely protected from the late-phase reduction in food intake and associated body weight loss (Extended Data Fig. 1a and b), demonstrating that conventional T cells are required for the late anorexic response. We then dissected the relative contributions of CD4$^+$ and CD8$^+$ T cells. Selective depletion of CD8$^+$, but not CD4$^+$, T cells substantially restored food intake and prevented the associated body weight loss (Extended Data Fig. 1c and d), consistent with previous reports and identifying CD8$^+$ T cells as the dominant T-cell population associated with LCMV-induced anorexia[29]. We then asked whether this response was specifically linked to antigen recognition by antiviral CD8$^+$ T cells. To distinguish antigen specificity, we adoptively transferred LCMV-specific P14 CD8$^+$ T cells or irrelevant OT-I CD8$^+$ T cells into *Tcra*$^{-/-}$ mice before LCMV infection. Strikingly, only transfer of P14 cells, but not irrelevant CD8$^+$ T cells, restored the late-phase anorexic response in *Tcra*$^{-/-}$ mice (Extended Data Fig. 1e and f). Thus, extending previous observations that CD8$^+$ T cells contribute to LCMV-associated anorexia, our findings demonstrate that the late-phase suppression of feeding is specifically associated with an antigen-specific antiviral CD8$^+$ T-cell response. These results further raised the possibility that antigen-specific adaptive immunity may engage the nervous system to regulate feeding behavior during viral infection.

Antiviral CD8$^+$ T-cell immunity engages a NTS-PB circuit to suppress feeding

Because feeding behavior is centrally regulated by the nervous system, we next sought to identify

the brain regions recruited during the late-phase anorexic response. Whole-brain tissue clearing followed by three-dimensional mapping of c-Fos expression at days 6-7 after LCMV infection, when food intake reached its nadir, revealed widespread neuronal activation across multiple brain regions (Fig. 1d and Video S1). Among these regions, the nucleus of the solitary tract (NTS) and parabrachial nucleus (PB), two interconnected structures that integrate visceral and internal-state signals and regulate feeding behavior[16,17,31], exhibited particularly prominent neuronal recruitment following viral infection. Histological analysis confirmed a marked increase in c-Fos$^+$ neurons in both the NTS and PB during the late anorexic phase (Fig. 1e and f). Importantly, neuronal activity in both regions closely tracked the dynamics of anorexia, increasing as food intake declined and diminishing as feeding recovered (Extended Data Fig. 1g and h). Thus, the NTS-PB axis represents a prominent neural correlate of late-phase anorexia during LCMV infection.

Given the dependence of late-phase anorexia on antigen-specific CD8$^+$ T cells, we next asked whether recruitment of the NTS-PB circuit was similarly linked to the antiviral CD8$^+$ T-cell response. We examined c-Fos expression in *Tcra*$^{-/-}$ mice and in wild-type mice selectively depleted of CD4$^+$ or CD8$^+$ T cells. Consistent with the behavioral phenotype, neuronal activation in both the NTS and PB was markedly reduced in *Tcra*$^{-/-}$ mice and in CD8$^+$ T cell-depleted wild-type mice, whereas CD4$^+$ T-cell depletion had little effect (Fig. 1g-j). Moreover, adoptive transfer of antigen-specific P14 CD8$^+$ T cells into *Tcra*$^{-/-}$ mice restored neuronal activation following LCMV infection (Extended Data Fig. 1i and j). Thus, antigen-specific CD8$^+$ T-cell immunity is closely associated with activation of brainstem feeding circuits, providing a potential neural link between adaptive antiviral immunity and neuronal activity in brainstem.

We next asked whether activation of the NTS neuronal ensemble recruited during peak anorexia was sufficient to suppress feeding. To selectively manipulate this infection-associated neuronal population, we injected a Cre-dependent excitatory hM3Dq or control adeno-associated virus (AAV) into the NTS of Fos-CreER;Ai14 mice. Two weeks later, mice were infected with LCMV, and 4-hydroxytamoxifen (4-OHT) was administered on day 6, to genetically label neurons activated during this phase and drive selective expression of hM3Dq in the corresponding NTS ensemble (Fig. 1k). After food intake had fully recovered, chemogenetic reactivation of this infection-associated neuronal ensemble induced a pronounced reduction in food intake accompanied by acute body weight loss, whereas reactivation of control-treated animals had no comparable effect (Fig. 1l-n). These findings demonstrate that the NTS neuronal ensemble recruited during peak LCMV-induced anorexia is sufficient to reproduce the anorexic phenotype.

Excitatory Vglut2$^+$ neurons in the NTS mediate LCMV-induced anorexia

The late-phase anorexic response to LCMV is dependent on antigen-specific antiviral CD8$^+$ T-cell immunity. This dependence on adaptive immune memory presents a challenge for directly testing the necessity of the infection-recruited NTS neuronal ensemble using a conventional ablation-and-re-challenge strategy, because viral re-exposure would elicit a secondary immune response that is fundamentally different from the primary response. We therefore sought to define the cellular identity of the NTS neurons recruited during LCMV-induced anorexia as a first step toward identifying the neuronal population that functionally controls feeding suppression.

The NTS contains a highly heterogeneous neuronal population comprising both Vglut2$^+$ excitatory and Vgat$^+$ inhibitory neurons, with multiple molecularly defined subtypes within both

compartments[31-33]. To determine the neuronal populations preferentially recruited during the late anorexic phase of LCMV infection, we generated Vglut2-Cre;Ai14 and Vgat-Cre;Ai14 mice and examined the overlap between genetically labeled neuronal populations and c-Fos expression. Strikingly, the vast majority of c-Fos$^+$ NTS neurons were Vglut2$^+$ excitatory neurons, whereas only a small fraction was Vgat$^+$ inhibitory neurons (Fig. 2a and b). Thus, LCMV-induced anorexia preferentially recruits excitatory rather than inhibitory neurons within the NTS. We next asked whether the activated Vglut2$^+$ neurons could be further resolved into specific molecularly defined subpopulations. Among the major Vglut2$^+$ NTS neuronal populations, including Phox2b$^+$, Adcyap1$^+$, and Th$^+$ neurons, Phox2b$^+$ neurons accounted for approximately 55% of the c-Fos$^+$ population, whereas only a small proportion of c-Fos$^+$ neurons expressed Adcyap1 or Th (Fig. 2c-e and Extended Data Fig. 2a). These findings reveal a marked molecular bias in the NTS neuronal response to LCMV infection, with the late anorexic state preferentially recruiting Vglut2$^+$ excitatory neurons and, within this population, a prominent Phox2b$^+$ neuronal subset.

To identify the functionally relevant neuronal compartment within the NTS, we first compared the contributions of excitatory Vglut2$^+$ and inhibitory Vgat$^+$ neurons. We delivered Cre-dependent inhibitory hM4Di to the NTS of Vglut2-Cre or Vgat-Cre mice before LCMV infection and selectively silenced the targeted populations with CNO on day 6 post infection, coinciding with the peak of anorexia (Fig. 2f). Acute inhibition of Vglut2$^+$ neurons produced a rapid and substantial restoration of food intake and markedly attenuated body weight loss (Fig. 2g-j). In contrast, inhibition of Vgat$^+$ neurons had little effect on either food intake or body weight (Fig. 2k-n). These findings identify excitatory Vglut2$^+$ neurons as the principal functional compartment within the NTS that sustains LCMV-induced late phase anorexia.

We next asked whether the anorexigenic activity of Vglut2$^+$ neurons could be attributed to a single molecularly defined excitatory subtype. Given the preferential recruitment of Phox2b$^+$ neurons among LCMV-activated NTS neurons, we selectively inhibited this population using chemogenetic hM4Di. Inhibition of Phox2b$^+$ neurons partially restored food intake and attenuated body weight loss (Extended Data Fig. 2b-f), demonstrating that this population may contribute to the anorexic response. However, the magnitude of rescue was substantially less than that achieved by broader inhibition of Vglut2$^+$ neurons. This incomplete rescue argues against Phox2b$^+$ neurons acting as the sole excitatory substrate for LCMV-induced anorexia and instead suggests that the anorexigenic signal is distributed across multiple distinct Vglut2$^+$ NTS populations. Consistent with this interpretation, selective inhibition of Adcyap1$^+$ or TH$^+$ neurons had no appreciable effect on food intake or body weight (Extended Data Fig. 2g-n). Thus, rather than being encoded by a single molecularly defined neuronal subtype, LCMV-induced anorexia is supported by a distributed excitatory Vglut2$^+$ NTS ensemble, with Phox2b$^+$ neurons representing one functionally relevant component of this broader circuit.

Virus-specific CD8$^+$ T cells induce sympathetic nerve injury to drive infection-associated anorexia

LCMV infects a broad range of cell types, including immune, stromal, epithelial, and glial cells, across multiple tissues such as the spleen, liver, lung, and brain[34,35]. We therefore first asked whether direct viral infection within the central nervous system might provide a local trigger for CD8$^+$ T-cell recruitment and neuronal activation. To address this possibility, we transferred GFP-labeled P14

cells into wild-type mice and visualized LCMV-infected cells together with $CD8^+$ T cells in the brainstem, where we had observed prominent neuronal activation during the late anorexic phase (Fig. 3a). At day 6 post infection, very few LCMV-infected cells and $CD8^+$ T cells were detected within this region (Extended Data Fig. 3a), arguing against substantial local infiltration of antiviral $CD8^+$ T cells into the brainstem as the primary mechanism linking adaptive immunity to anorexia.

We therefore asked whether antiviral $CD8^+$ T cells might instead interact with virus-infected neural or glial elements in peripheral tissues. We examined the spatial distribution of LCMV-infected cells, P14 cells, and neural and glial structures in the spleen and liver. Notably, immunofluorescence analysis revealed LCMV infection of $S100B^+$ glial cells in both organs (Fig. 3b and c), accompanied by a reduction in the abundance of glial cells compared with uninfected controls. This observation is consistent with previous reports identifying peripheral glial cells, including Schwann cells, as targets of LCMV infection[36]. Strikingly, abundant antigen-specific P14 T cells were localized in close proximity to peripheral nerve fibers (Fig. 3b and c), suggesting preferential accumulation of antiviral $CD8^+$ T cells at peripheral neural structures. Together, these findings suggest that adaptive antiviral immunity may interface with the nervous system outside the CNS, creating a peripheral neuro-immune niche in which virus-infected neural-associated cells are juxtaposed with antigen-specific $CD8^+$ T cells. Such perineural localization provides a potential anatomical substrate through which peripheral antiviral immunity could perturb neural signaling and ultimately influence brainstem circuits controlling feeding behavior.

To determine whether antiviral adaptive immunity affects the peripheral nervous system during LCMV infection, we performed three-dimensional imaging of splenic innervation using the pan-neuronal marker PGP9.5 and the sympathetic neuronal marker tyrosine hydroxylase (TH), respectively. Strikingly, LCMV infection induced extensive loss and retraction of sympathetic nerve fibers throughout the spleen (Fig. 3d, e, Extended Data Fig. 3b, c and Video S2). Because the cell bodies of splenic sympathetic neurons reside primarily in the celiac ganglion (CG)[37], we next examined neuronal injury in the CG by assessing expression of activating transcription factor 3 (ATF3), a well-established molecular marker of peripheral neuronal stress[38]. Consistent with the extensive loss of TH^+ sympathetic innervation in the spleen, LCMV infection induced robust ATF3 expression in sympathetic neuronal somata within the CG (Fig. 3f and g), indicating that viral infection was associated with substantial injury to the splenic sympathetic nervous system. We next asked whether this peripheral sympathetic nerve injury depended on the antiviral adaptive immune response. Infected *Tcra*$^{-/-}$ mice preserved the TH^+ sympathetic innervation in the spleen and exhibited rare ATF3 induction in the CG, whereas reconstitution with P14 $CD8^+$ T cells restored both the loss of splenic TH^+ fibers and the induction of ATF3 in sympathetic neuronal somata (Fig. 3h-k). Similarly, depletion of $CD8^+$ T cells, but not $CD4^+$ T cells, prevented the denervation of sympathetic nerve in the spleen and the stress response in celiac ganglion following LCMV infection (Extended Data Fig. 3d-g). Together, these findings demonstrate that LCMV-induced injury of the peripheral sympathetic nervous system is strongly dependent on adaptive antiviral $CD8^+$ T-cell immunity, with antigen-specific $CD8^+$ T cells being sufficient to recapitulate sympathetic nerve loss and neuronal stress.

Given that antiviral $CD8^+$ T-cell immunity is associated with both peripheral sympathetic nerve injury and suppression of feeding, we next asked whether sympathetic nerve injury represents a functional link between the antiviral immune response and anorexia. To determine whether perturbation of the peripheral sympathetic nervous system is sufficient to engage the anorexia-

associated neural circuit, we treated wild-type mice with 6-hydroxydopamine (6-OHDA) to selectively lesion peripheral sympathetic fibers (Extended Data Fig. 3h). Acute sympathetic denervation induced a rapid reduction in food intake accompanied by body weight loss during the first 2 days after treatment (Fig. 3l and m). Notably, 6-OHDA treatment also elicited robust neuronal activation in both the NTS and PB (Fig. 3n and o), recapitulating key features of the behavioral and brainstem neuronal responses observed during LCMV infection. These findings suggested that disruption of peripheral sympathetic innervation is sufficient to engage the neural circuitry associated with infection-induced anorexia.

We next asked whether sympathetic denervation is required for the anorexic response to LCMV infection. Mice were pretreated with 6-OHDA to ablate peripheral sympathetic fibers and allowed to recover before LCMV infection (Fig. 3p). Strikingly, mice with established sympathetic denervation were largely protected from the reduction in food intake and associated body weight loss following LCMV infection (Fig. 3q and r). Thus, sympathetic denervation not only recapitulated key features of the anorexic response but, when established before infection, substantially attenuated LCMV-induced feeding suppression. Together, these findings identify the peripheral sympathetic nervous system as a critical functional intermediary linking antiviral T-cell immunity to neural circuits that regulate feeding behavior.

Vagal afferents relay peripheral injury signals to the NTS and mediate anorexia

Peripheral sympathetic nerve injury was sufficient to activate the NTS and PB and was required for LCMV-induced feeding suppression. We next sought to determine how peripheral neural injury signals are transmitted to the brainstem. The NTS is a major recipient of visceral sensory information conveyed by vagal afferents, which continuously monitor the physiological state of peripheral organs and relay signals associated with tissue perturbation to the brain[39,40]. We therefore hypothesized that the vagus nerve might provide an ascending pathway linking peripheral immune-associated neural injury to anorexigenic brainstem circuits.

To test this possibility, we first examined vagal sensory neuron activation following LCMV infection. During the late anorexic phase, LCMV infection induced a marked increase in c-Fos expression in Phox2b$^+$ neurons within the nodose ganglion (NG) (Fig. 4a and b), the cell body region of vagal sensory afferents[41]. This activation coincided with peripheral sympathetic nerve injury and robust neuronal activation in the NTS and PB, suggesting coordinated recruitment of a peripheral-vagal-brainstem axis during late-phase anorexia. Furthermore, 6-OHDA-mediated sympathetic denervation also elicited substantial activation of vagal sensory neurons (Fig. 4c and d), further linking sympathetic nerve injury to vagal afferent activity. We next directly tested the functional contribution of vagal signaling by performing bilateral subdiaphragmatic vagotomy before LCMV infection. Compared with sham-operated controls, vagotomized mice exhibited substantially attenuated body weight loss and markedly preserved food intake following LCMV challenge (Fig. 4e and f). Meanwhile, vagotomy also markedly reduced LCMV-induced c-Fos expression in Phox2b$^+$ NG neurons (Fig. 4g and h) and substantially diminished neuronal activation in both the NTS and PB (Fig. 4i and j). Thus, vagal sensory signaling is engaged during LCMV-induced anorexia and provides an important ascending pathway linking peripheral neural perturbation to brainstem feeding circuits.

IL-33-ST2-MyD88 signaling links antiviral immunity to late-phase anorexia

Having established that a peripheral nerve injury-vagal-brainstem pathway links antiviral adaptive immunity to late-phase anorexia, we next sought to identify the immune signals that engage this neural axis during LCMV infection. Several cytokines, including type I interferons (IFN-Is), IL-12, IL-6, and IL-33, have been implicated in shaping antiviral $CD8^+$ T-cell responses during LCMV infection[26,42-44]. We therefore examined whether these cytokine pathways contribute to the anorexic response using genetic deficiency or antibody-mediated blockade. Disruption of IFN-I signaling selectively attenuated the modest reduction in food intake and body weight during the early phase of infection, but did not prevent the subsequent development of profound anorexia and weight loss during days 6-8 post infection (Extended Data Fig. 4a and b). Consistent with the persistence of the late behavioral phenotype, neuronal activation in both the NTS and PB remained robust in *Ifnar*$^{-/-}$ mice (Extended Data Fig. 4c and d). Likewise, genetic deficiency of IL-6 or blockade of IL-12/23 signaling failed to protect against late-phase anorexia or associated weight loss (Extended Data Fig. 4e-h). Thus, although IFN-I signaling contributes to the initial suppression of feeding, neither type I IFN, IL-6, nor IL-12/23 signaling is required for the late-phase anorexic response.

Surprisingly, in contrast to these cytokine pathways, *Il1rl1*$^{-/-}$ mice, which lack ST2, were almost completely protected from the profound reduction in food intake and body weight during the late phase of LCMV infection, while retaining the early decrease in food intake (Fig. 5a and b). The behavioral protection was accompanied by a marked loss of neuronal activation in both the NTS and PB (Fig. 5c and d), indicating that ST2 signaling is required for recruitment of the brainstem circuit associated with late-phase anorexia. Notably, ST2 deficiency also substantially preserved splenic sympathetic innervation and markedly reduced ATF3 induction in sympathetic neuronal somata within the celiac ganglion (Fig. 5e-h). Thus, disruption of IL-33-ST2 signaling simultaneously prevented peripheral sympathetic nerve injury and downstream brainstem activation, placing this pathway upstream of the peripheral neuroimmune circuit that couples LCMV infection to feeding suppression.

Because MyD88 serves as a central adaptor downstream of ST2[45,46], we next asked whether disruption of MyD88 signaling would phenocopy ST2 deficiency. Consistent with this possibility, *Myd88*$^{-/-}$ mice were strongly protected from late-phase anorexia and weight loss and exhibited markedly reduced neuronal activation in both the NTS and PB (Extended Data Fig. 5a-d). Interestingly, *Myd88*$^{-/-}$ mice also showed an attenuation of the modest reduction in food intake and body weight during the first 2 days of infection, resembling the early phenotype observed in *Ifnar*$^{-/-}$ mice (Extended Data Fig. 4a and b). These findings reveal a biphasic organization of LCMV-induced sickness behavior: an early, relatively mild suppression of feeding that is sensitive to innate inflammatory pathways involving MyD88 and type I IFNs, and a distinct late phase in which severe anorexia is associated with ST2-MyD88 signaling, peripheral sympathetic nerve injury, and recruitment of the NTS-PB circuit. Together, these results identify IL-33-ST2-MyD88 signaling as a critical immune pathway associated with the transition from an early innate sickness response to the profound late-phase anorexia that accompanies adaptive antiviral immunity.

$CD8^+$ T cell-intrinsic IL-33-ST2 signaling is essential for infection-associated anorexia

We next asked whether IL-33 acts directly on antiviral $CD8^+$ T cells to engage the peripheral

neuroimmune circuit and drive late-phase anorexia. We first examined the temporal expression of ST2 on $CD8^+$ T cells during LCMV infection. Analysis of published single-cell RNA-sequencing data[47] revealed that *Il1rl1* expression was transiently induced in $CD8^+$ T cells during the infection, with detectable expression at day 8 but little or no expression at baseline or day 15 (Extended Data Fig. 5e and f). Notably, this induction coincided with the emergence of profound late-phase anorexia, raising the possibility that IL-33 directly engages antiviral $CD8^+$ T cells during this phase of infection.

To directly test this possibility, we generated ST2-deficient, LCMV-specific P14 $CD8^+$ T cells by crossing *Il1rl1*$^{-/-}$ mice with P14 TCR-transgenic mice. Wild-type or ST2-deficient P14 cells were adoptively transferred into *Il1rl1*$^{-/-}$ recipients one day before LCMV infection, thereby selectively restoring ST2 expression in antigen-specific $CD8^+$ T cells. Strikingly, wild-type P14 cells restored the late-phase reduction in food intake and body weight loss in *Il1rl1*$^{-/-}$ recipients, whereas ST2-deficient P14 cells failed to do so (Fig. 5i and j). Consistent with the behavioral phenotype, only wild-type P14 cells restored neuronal activation in both the NTS and PB (Fig. 5k and l). To determine whether this requirement extended to the canonical downstream signaling pathway of ST2, we performed an analogous reconstitution experiment using wild-type or MyD88-deficient P14 cells into *Myd88*$^{-/-}$ recipients. Wild-type, but not MyD88-deficient, P14 cells reverted the anorexic response and NTS/PB neuronal activation (Extended Data Fig. 5g-j). Together, these complementary loss-of-function and reconstitution experiments establish that $CD8^+$ T cell-intrinsic IL-33-ST2-MyD88 signaling is required for antigen-specific antiviral immunity to engage the peripheral neuroimmune axis and activate anorexia-associated brainstem circuits during persistent viral infection.

$CX3CR1^+$ effector $CD8^+$ T cells engage the anorexia-associated neural circuit

Given our finding that $CD8^+$ T cell-intrinsic ST2-MyD88 signaling is required for LCMV-induced anorexia, we next asked whether this pathway promotes sickness behavior by shaping the differentiation state of antiviral $CD8^+$ T cells (Extended Data Fig. 6a). Consistent with previous observations[27], *Il1rl1*$^{-/-}$ mice exhibited an approximately threefold reduction in GP33-specific $CD8^+$ T cells in the spleen at day 6 after LCMV infection compared with wild-type mice (Fig. 6a). We therefore further resolved the GP33-specific $CD8^+$ T-cell compartment using TCF-1 and CX3CR1, which distinguish stem-like and effector-like populations, respectively[24,48]. Both $TCF\text{-}1^+$ stem-like and $CX3CR1^+$ effector-like GP33-specific $CD8^+$ T cells were markedly reduced in *Il1rl1*$^{-/-}$ mice, whereas the $TCF\text{-}1^-CX3CR1^-$ population was relatively preserved (Fig. 6a-c). These findings indicate that ST2 signaling substantially influences the differentiation and/or maintenance of antigen-specific $CD8^+$ T-cell populations during persistent viral infection.

We next asked whether the altered $CD8^+$ T-cell differentiation state in *Il1rl1*$^{-/-}$ mice could account for their protection from anorexia. Because type I interferon signaling has been reported to restrain the development of stem-like $CD8^+$ T cells, particularly under conditions of altered IL-33/ST2 signaling[27], we blocked IFN-I signaling in *Il1rl1*$^{-/-}$ mice using an IFNAR-blocking antibody (Extended Data Fig. 6b). IFNAR blockade substantially restored the $TCF\text{-}1^+$ stem-like $CD8^+$ T-cell population but had moderate effect on the frequency of $CX3CR1^+$ effector-like cells (Extended Data Fig. 6c and d). Importantly, however, restoration of the $TCF\text{-}1^+$ population failed to restore the reduction in food intake or body weight loss in *Il1rl1*$^{-/-}$ mice following LCMV infection (Extended

Data Fig. 6 e and f). Thus, the loss of stem-like CD8$^+$ T cells resulting from ST2 deficiency is not sufficient to explain the protection from late-phase anorexia.

To further test this possibility independently of ST2 signaling, we infected *CD4^{Cre}Tcf7$^{fl/fl}$* mice with LCMV, which selectively disrupted TCF-1 expression in T cells. Upon infection, these mice exhibited specific absence of Ly108$^+$ stem-like CD8$^+$ T-cell compartment, but reserved CX3CR1$^+$ effector-like population (Extended Data Fig. 6g and h). Meanwhile, they developed anorexia and body weight loss comparable to those observed in control animals (Extended Data Fig. 6i and j). Consistently, neuronal activation in the NTS and PB was preserved in the absence of TCF-1$^+$ stem-like CD8$^+$ T cells (Extended Data Fig. 6k and l). Together, these findings indicate that although IL-33-ST2 signaling profoundly shapes the differentiation state of antiviral CD8$^+$ T cells, the late-phase anorexic response is not determined by the abundance of TCF-1$^+$ stem-like CD8$^+$ T cells.

We next asked whether the CX3CR1$^+$ effector-like CD8$^+$ T-cell population was sufficient to engage the anorexigenic neural circuit. To directly compare the functional capacity of distinct antigen-specific CD8$^+$ T-cell states, we first transferred naïve P14 cells into *Tcra$^{-/-}$* mice one day before LCMV infection. On day 5 after infection, Ly108$^+$ stem-like, CX3CR1$^+$ effector-like, or CX3CR1$^-$Ly108$^-$ P14 cells were purified from infected donor mice and transferred into infection-matched *Tcra$^{-/-}$* recipients (Fig. 6d). Strikingly, transfer of CX3CR1$^+$ effector-like P14 cells restored the reduction of food intake and associated body weight loss, whereas neither Ly108$^+$ stem-like nor CX3CR1$^-$Ly108$^-$ P14 cells reproduced the anorexic phenotype (Fig. 6e-g). Consistent with the behavioral response, robust neuronal activation in both the NTS and PB was selectively restored in recipients of CX3CR1$^+$ effector-like cells (Fig. 6h, i and Extended Data Fig. 6m, n). These findings identify CX3CR1$^+$ effector-like antiviral CD8$^+$ T cells as a functionally competent population capable of engaging the anorexia-associated brainstem circuit. Together with the preceding analyses, these results suggest that IL-33-ST2 signaling contributes to suppression of feeding behavior not simply by regulating the abundance or differentiation of antiviral CD8$^+$ T cells, but by sustaining a functionally specialized effector state that couples antigen-specific immunity to neural activation.

Perforin-dependent effector function links antiviral CD8$^+$ T cells to anorexia

Finally, we sought to define the effector mechanisms through which antiviral CD8$^+$ T cells engage the peripheral neuroimmune pathway to suppress feeding. Effector CD8$^+$ T cells can influence tissue physiology through the production of inflammatory cytokines, including IFN-γ and TNF, or through direct cytolytic activity mediated by perforin and granzymes[18,49]. We therefore first examined whether inflammatory cytokines were required for the anorexic response. Mice deficient in IFN-γ or TNF receptor signaling developed anorexia and body weight loss comparable to those of wild-type controls following LCMV infection (Extended Data Fig. 7a-d). Thus, under physiological conditions, neither IFN-γ nor TNF signaling is required for the severe late-phase anorexia induced by LCMV infection.

We next examined the contribution of cytolytic effector function. Loss of either granzyme B or perforin partially attenuated the reduction in food intake and body weight during peak anorexia (Fig. 6j-m), implicating perforin-granzyme-dependent cytotoxicity as an important effector mechanism. The relatively modest protection observed in *Prf1$^{-/-}$* mice, however, was unexpected given the prominent contribution of cytotoxicity and raised the possibility that loss of perforin may trigger compensatory inflammatory responses that obscure the behavioral consequence of impaired

cytolysis[50,51]. Consistent with this possibility, serum IFN-γ, but not TNF, was elevated more than 10-fold in LCMV-infected *Prf1*$^{-/-}$ mice compared with infected wild-type controls (Extended Data Fig. 7e). Neutralization of IFN-γ in *Prf1*$^{-/-}$ mice resulted in substantially greater recovery of food intake and attenuation of body weight loss than perforin deficiency alone (Fig. 6n-p). These findings reconcile the partial protection conferred by perforin deficiency with the dispensability of physiological IFN-γ signaling: although IFN-γ is not required for CD8$^+$ T cell-mediated anorexia under normal conditions, excessive IFN-γ production that accumulates when cytolytic function is impaired can provide an additional, pathological signal capable of exacerbating sickness behavior. Together, these findings identify perforin-dependent cytotoxicity as a major effector mechanism through which antiviral CD8$^+$ T cells drive late-phase anorexia. Combined with the preceding results, we define a continuous neuroimmune pathway in which antigen-specific CD8$^+$ T cells, conditioned by cell-intrinsic IL-33-ST2-MyD88 signaling, engage perforin-dependent effector activity associated with peripheral sympathetic nerve injury; the resulting peripheral neural perturbation is transmitted through vagal afferents to excitatory NTS circuits, ultimately coupling antiviral immunity to suppression of feeding.

Discussion

Infection-associated anorexia has traditionally been attributed to innate inflammatory responses, but accumulating evidence suggests that adaptive immunity also contributes to the regulation of feeding behavior[1,28,29,52]. Here, we identify an unappreciated neuro-immune mechanism through which antiviral CD8$^+$ T-cell responses engage the brainstem to suppress food intake during LCMV infection. We demonstrate that IL-33-ST2-MyD88 signaling promotes the anorexigenic activity of antiviral CD8$^+$ T cells, which is associated with peripheral sympathetic nerve injury and subsequent engagement of vagal afferents that relay signals to Vglut2$^+$ neurons in the NTS. These findings establish a peripheral-to-brain neuro-immune axis that couples adaptive antiviral immunity to behavioral regulation.

Anorexia is a highly conserved physiological response to infection, yet the relative contributions of innate and adaptive immunity to its induction remain incompletely understood[29,53]. Previous studies have implicated inflammatory cytokines, including IL-1, TNF, IL-6, and GDF15, as well as lipid mediators such as PGE_2 and various neurotransmitters, in the suppression of food intake[5,8,12,54]. Our findings extend this framework by revealing distinct temporal and immunological phases of anorexia during LCMV infection. The early, transient reduction in food intake may result from the rapid induction of IFN-Is, whereas the delayed and more pronounced anorexia parallels the expansion and effector differentiation of virus-specific CD8$^+$ T cells. The resistance of T cell-deficient mice to late-phase anorexia, together with the restoration of this phenotype by adoptive transfer of LCMV-specific P14 CD8$^+$ T cells, provides direct evidence that antigen-specific adaptive immunity contributes to infection-associated anorexia. Notably, this phenomenon is not restricted to viral infection. Infection with the protozoan parasite *Trypanosoma brucei* has also been shown to induce anorexia through activation of CD4$^+$ and CD8$^+$ T-cell responses, suggesting that adaptive immune-driven sickness behavior may represent a broader physiological response to persistent infection[52]. Together, these findings support a model in which sickness-associated anorexia evolves from an early innate inflammatory response to a later adaptive immune-dependent response, linking the temporal progression of host immunity to coordinated changes in feeding behavior.

Our findings identify IL-33-ST2-MyD88 signaling as an important regulator of the anorexigenic activity of antiviral $CD8^+$ T cells. Although IL-33 is widely recognized as an alarmin that promotes type 2 immunity and tissue repair, its role in shaping antiviral T cell-associated behavioral responses has received considerably less attention[46,55]. Consistent with previous studies, reanalysis of published scRNA-seq data revealed that ST2 expression on virus-specific $CD8^+$ T cells is transiently increased during the late phase of anorexia[47]. Importantly, ST2 deficiency impaired the ability of antiviral $CD8^+$ T cells to induce anorexia and activate neurons in the NTS and PB, which coincided with a reduction in the abundance of antigen-specific $CD8^+$ T cells, including both $Tcf1^+$ stem-like and $CX3CR1^+$ effector-like populations. Although blockade of type I interferon signaling restored the $Tcf1^+$ stem-like population in ST2-deficient mice, it did not rescue anorexia, indicating that altered T-cell abundance alone is insufficient to explain the behavioral phenotype. Notably, $CX3CR1^+$ effector-like $CD8^+$ T cells, but not $Ly108^+$ stem-like or $CX3CR1^-Ly108^-$ populations, were sufficient to restore anorexia and brainstem neuronal activation upon adoptive transfer into infection-matched T cell-deficient animals, highlighting functional heterogeneity among antiviral $CD8^+$ T-cell subsets and implicating effector differentiation in the coupling of adaptive immunity to behavioral regulation. We further found that IFN-γ and TNF signaling were dispensable for LCMV-induced anorexia, arguing against a requirement for these canonical inflammatory cytokines in this behavioral response. In contrast, genetic disruption of perforin or granzyme B conferred partial protection from anorexia, implicating cytotoxic effector activity in this response. Together, these findings suggest that the anorexigenic function of antiviral $CD8^+$ T cells is more closely associated with their cytotoxic effector state than with classical cytokine-mediated inflammation. Thus, IL-33-ST2-MyD88 signaling may couple inflammatory tissue cues to the generation and functional programming of specialized effector $CD8^+$ T cells with neuro-immune regulatory activity.

An important finding of this study is the involvement of peripheral neural pathways in translating antiviral adaptive immunity into altered feeding behavior, distinguishing this mechanism from that associated with primary intracranial infection[56]. Following intravenous LCMV infection, very few antigen-specific $CD8^+$ T cells infiltrated the CNS, making direct engagement of NTS neurons by antiviral T cells unlikely. Instead, we observed recruitment of antigen-specific $CD8^+$ T cells to sympathetic nerve fibers in the spleen and liver. Consistent with previous reports, Schwann cells were also infected by LCMV[36], raising the possibility that infected peripheral glial cells or other nerve-associated cells may provide a target or interface for antiviral T-cell responses. Correspondingly, LCMV infection was associated with structural changes in splenic sympathetic nerves, accompanied by neuronal stress responses in the celiac ganglion. These changes were dependent on adaptive $CD8^+$ T-cell immunity and IL-33 signaling, as they were markedly attenuated in T cell-deficient or ST2-deficient mice and restored by adoptive transfer of antigen-specific $CD8^+$ T cells. The association between sympathetic nerve remodeling and anorexia, together with the attenuation of anorexia by sympathetic denervation before infection, provides functional evidence that peripheral sympathetic pathways contribute to antiviral immunity-associated behavioral changes. In parallel, vagotomy reduced infection-induced anorexia, while increased neuronal activation in the nodose ganglion following infection further implicated vagal afferent signaling in this response. Together, these findings support a model in which adaptive antiviral immunity engages peripheral autonomic circuits, involving both sympathetic and vagal pathways, to relay infection-associated tissue perturbations to brainstem feeding circuits. An important unresolved question is how vagal afferents detect or integrate signals arising from sympathetic nerve injury.

Potential mechanisms may involve local inflammatory mediators, extracellular ATP or other damage-associated signals, or neuro-glial interactions, which need further investigation[39,57].

The NTS is a central brainstem hub that integrates peripheral immune, metabolic, and visceral signals to regulate feeding and sickness behavior. Located within the dorsal vagal complex, the NTS receives diverse visceral and inflammatory inputs and engages downstream circuits that control anorexia and food avoidance[58,59]. Innate inflammatory and tissue-stress signals, including LPS, GDF15, and infection-associated sensory cues, activate distinct NTS populations, including ADCYAP1$^+$ and GFRAL$^+$ neurons, and can drive anorexia and sickness behavior[12,14,31,60,61]. NTS glutamatergic neurons further engage the lateral PB, including anorexigenic CGRP$^+$ neurons, whereas PB outputs to the central amygdala (CeA) contribute to appetite suppression and food avoidance[16,17]. Our findings extend this established neuro-immune framework by identifying adaptive antiviral immunity as an upstream regulator of the NTS feeding circuit. Whereas previous studies have largely linked NTS activation to rapid innate inflammatory or tissue-stress signals, we demonstrate that antigen-specific CD8$^+$ T-cell responses during LCMV infection engage Vglut2$^+$ NTS neurons and drive anorexia. This finding reveals that the NTS is not restricted to sensing acute innate inflammatory states but can also integrate signals generated by an evolving antigen-specific immune response. Thus, the NTS may represent a common neural convergence point through which temporally distinct arms of immunity-early innate inflammation and later adaptive antiviral responses-are translated into behavioral adaptations. Our study therefore establishes a previously unappreciated connection between antigen-specific T-cell immunity and a conserved brainstem feeding circuit, providing a mechanistic framework for how adaptive immune responses can directly shape host behavior during infection.

The identification of a CD8$^+$ T cell-dependent peripheral-brainstem axis raises important questions about the physiological significance of infection-associated anorexia. Reduced food intake is accompanied by a metabolic transition from glucose utilization toward lipid mobilization, suggesting that anorexia may represent an adaptive metabolic response that reshapes host physiology during infection[3,62]. The consequences of this metabolic switch, however, may depend on the nature and stage of infection. Indeed, glucose utilization has been reported to support host survival during influenza infection, whereas excessive glucose availability can exacerbate systemic inflammation and mortality in bacterial infection[3]. Conversely, emerging evidence suggests that lipid availability can directly influence antiviral CD8$^+$ T-cell differentiation, promoting stem-like populations while limiting terminal exhaustion during persistent LCMV infection[63]. These observations raise the possibility that infection-associated anorexia may not simply be a consequence of immune activation, but could feed back onto the immune response by altering systemic nutrient availability. Intriguingly, unpublished observations further suggest that activation of DBH$^+$ neurons in the NTS can restrain effector CD8$^+$ T-cell activity, thereby limiting tissue hemorrhage and improving survival. Together, these findings raise the possibility of a reciprocal neuro-immune circuit in which antiviral CD8$^+$ T cells engage peripheral neural pathways to suppress feeding, while the resulting metabolic and neural adaptations subsequently modulate CD8$^+$ T-cell effector function and tissue injury. Such a circuit could provide a mechanism for coordinating the intensity of adaptive immunity with the metabolic state and tissue tolerance of the host during infection.

In summary, our study identifies a neuro-immune pathway through which antigen-specific CD8$^+$ T-cell responses regulate feeding behavior during LCMV infection. By linking IL-33-ST2-dependent

effector T-cell responses to peripheral autonomic pathways and NTS neuronal activity, our findings expand the understanding of how adaptive immunity communicates with the nervous system. This work establishes the peripheral-brainstem axis as an important component of infection-associated behavioral regulation and highlights a broader principle whereby adaptive immune responses can actively shape host behavior through peripheral neural circuits. Understanding the molecular and cellular mechanisms governing this communication may provide new insights into how antiviral immunity, behavioral adaptation, metabolic homeostasis, and tissue tolerance are coordinated during infection.

References

1 Dantzer, R., O'Connor, J. C., Freund, G. G., Johnson, R. W. & Kelley, K. W. From inflammation to sickness and depression: when the immune system subjugates the brain. *Nature Reviews Neuroscience* **9**, 46–56 (2008). https://doi.org/10.1038/nrn2297

2 Medzhitov, R., Schneider, D. S. & Soares, M. P. Disease tolerance as a defense strategy. *Science* **335**, 936–941 (2012). https://doi.org/10.1126/science.1214935

3 Wang, A. *et al.* Opposing Effects of Fasting Metabolism on Tissue Tolerance in Bacterial and Viral Inflammation. *Cell* **166**, 1512–1525.e1512 (2016). https://doi.org/10.1016/j.cell.2016.07.026

4 Osterhout, J. A. *et al.* A preoptic neuronal population controls fever and appetite during sickness. *Nature* **606**, 937–944 (2022). https://doi.org/10.1038/s41586-022-04793-z

5 Dantzer, R. & Kelley, K. W. Twenty years of research on cytokine-induced sickness behavior. *Brain Behav Immun* **21**, 153–160 (2007). https://doi.org/10.1016/j.bbi.2006.09.006

6 Kelley, K. W. *et al.* Cytokine-induced sickness behavior. *Brain Behav Immun* **17 Suppl 1**, S112–118 (2003). https://doi.org/10.1016/s0889-1591(02)00077-6

7 Exton, M. S. Infection-induced anorexia: active host defence strategy. *Appetite* **29**, 369–383 (1997). https://doi.org/10.1006/appe.1997.0116

8 Langhans, W. Anorexia of infection: current prospects. *Nutrition* **16**, 996–1005 (2000). https://doi.org/10.1016/s0899-9007(00)00421-4

9 Baazim, H., Antonio-Herrera, L. & Bergthaler, A. The interplay of immunology and cachexia in infection and cancer. *Nature Reviews Immunology* **22**, 309–321 (2022). https://doi.org/10.1038/s41577-021-00624-w

10 Reardon, C., Murray, K. & Lomax, A. E. Neuroimmune Communication in Health and Disease. *Physiol Rev* **98**, 2287–2316 (2018). https://doi.org/10.1152/physrev.00035.2017

11 Kovacs, M., Dominguez-Belloso, A., Ali-Moussa, S. & Deczkowska, A. Immune control of brain physiology. *Nature Reviews Immunology* **25**, 515–527 (2025). https://doi.org/10.1038/s41577-025-01129-6

12 Hsu, J.-Y. *et al.* Non-homeostatic body weight regulation through a brainstem-restricted receptor for GDF15. *Nature* **550**, 255–259 (2017). https://doi.org/10.1038/nature24042

13 Zhu, X. A. *et al.* A neuroimmune circuit mediates cancer cachexia-associated apathy. *Science* **388**, eadm8857 (2025). https://doi.org/10.1126/science.adm8857

14 Bin, N. R. *et al.* An airway-to-brain sensory pathway mediates influenza-induced sickness. *Nature* **615**, 660–667 (2023). https://doi.org/10.1038/s41586-023-05796-0

15 Huerta, T. S. *et al.* Neural representation of cytokines by vagal sensory neurons. *Nature*

Communications **16**, 3840 (2025). https://doi.org/10.1038/s41467-025-59248-6

16 Wu, Q., Clark, M. S. & Palmiter, R. D. Deciphering a neuronal circuit that mediates appetite. *Nature* **483**, 594–597 (2012). https://doi.org/10.1038/nature10899

17 Carter, M. E., Soden, M. E., Zweifel, L. S. & Palmiter, R. D. Genetic identification of a neural circuit that suppresses appetite. *Nature* **503**, 111–114 (2013). https://doi.org/10.1038/nature12596

18 Barry, M. & Bleackley, R. C. Cytotoxic T lymphocytes: all roads lead to death. *Nature Reviews Immunology* **2**, 401–409 (2002). https://doi.org/10.1038/nri819

19 Im, S. J. *et al.* Defining CD8+ T cells that provide the proliferative burst after PD-1 therapy. *Nature* **537**, 417–421 (2016). https://doi.org/10.1038/nature19330

20 He, R. *et al.* Follicular CXCR5-expressing CD8+ T cells curtail chronic viral infection. *Nature* **537**, 412–416 (2016). https://doi.org/10.1038/nature19317

21 Ahmed, R. *et al.* New insights into progenitor exhausted T cell populations. *Nature Reviews Immunology* (2026). https://doi.org/10.1038/s41577-026-01328-9

22 Beltra, J.-C. *et al.* Developmental Relationships of Four Exhausted CD8+ T Cell Subsets Reveals Underlying Transcriptional and Epigenetic Landscape Control Mechanisms. *Immunity* **52**, 825–841.e828 (2020). https://doi.org/10.1016/j.immuni.2020.04.014

23 Sun, Q. & Dong, C. Regulators of CD8+ T cell exhaustion. *Nature Reviews Immunology* **26**, 129–151 (2026). https://doi.org/10.1038/s41577-025-01221-x

24 Wu, T. *et al.* The TCF1-Bcl6 axis counteracts type I interferon to repress exhaustion and maintain T cell stemness. *Sci Immunol* **1** (2016). https://doi.org/10.1126/sciimmunol.aai8593

25 Zander, R. *et al.* Tfh-cell-derived interleukin 21 sustains effector CD8(+) T cell responses during chronic viral infection. *Immunity* **55**, 475–493.e475 (2022). https://doi.org/10.1016/j.immuni.2022.01.018

26 Bonilla, W. V. *et al.* The alarmin interleukin-33 drives protective antiviral $CD8^+$ T cell responses. *Science* **335**, 984–989 (2012). https://doi.org/10.1126/science.1215418

27 Marx, A.-F. *et al.* The alarmin interleukin-33 promotes the expansion and preserves the stemness of Tcf-1+ CD8+ T cells in chronic viral infection. *Immunity* **56**, 813–828.e810 (2023). https://doi.org/10.1016/j.immuni.2023.01.029

28 Baazim, H. *et al.* CD8+ T cells induce cachexia during chronic viral infection. *Nature Immunology* **20**, 701–710 (2019). https://doi.org/10.1038/s41590-019-0397-y

29 Labarta-Bajo, L. *et al.* CD8 T cells drive anorexia, dysbiosis, and blooms of a commensal with immunosuppressive potential after viral infection. *Proc Natl Acad Sci U S A* **117**, 24998–25007 (2020). https://doi.org/10.1073/pnas.2003656117

30 McCusker, R. H. & Kelley, K. W. Immune–neural connections: how the immune system's response to infectious agents influences behavior. *Journal of Experimental Biology* **216**, 84–98 (2013). https://doi.org/10.1242/jeb.073411

31 Ilanges, A. *et al.* Brainstem ADCYAP1+ neurons control multiple aspects of sickness behaviour. *Nature* **609**, 761–771 (2022). https://doi.org/10.1038/s41586-022-05161-7

32 Holt, M. K. The ins and outs of the caudal nucleus of the solitary tract: An overview of cellular populations and anatomical connections. *J Neuroendocrinol* **34**, e13132 (2022). https://doi.org/10.1111/jne.13132

33 Gasparini, S., Almeida-Pereira, G., Munuzuri, A. S. P., Resch, J. M. & Geerling, J. C.

Molecular Ontology of the Nucleus of Solitary Tract. *J Comp Neurol* **532**, e70004 (2024). https://doi.org/10.1002/cne.70004

34 Mueller, S. N. *et al.* Viral targeting of fibroblastic reticular cells contributes to immunosuppression and persistence during chronic infection. *Proc Natl Acad Sci U S A* **104**, 15430–15435 (2007). https://doi.org/10.1073/pnas.0702579104

35 Lauterbach, H., Truong, P. & McGavern, D. B. Clearance of an immunosuppressive virus from the CNS coincides with immune reanimation and diversification. *Virology Journal* **4**, 53 (2007). https://doi.org/10.1186/1743-422X-4-53

36 Rambukkana, A., Kunz, S., Min, J., Campbell, K. P. & Oldstone, M. B. Targeting Schwann cells by nonlytic arenaviral infection selectively inhibits myelination. *Proc Natl Acad Sci U S A* **100**, 16071–16076 (2003). https://doi.org/10.1073/pnas.2232366100

37 Moura, M. *et al.* Macro- and Microanatomy of the Sympathetic Innervation of the Spleen in Rodents. *J Comp Neurol* **533**, e70086 (2025). https://doi.org/10.1002/cne.70086

38 Tsujino, H. *et al.* Activating Transcription Factor 3 (ATF3) Induction by Axotomy in Sensory and Motoneurons: A Novel Neuronal Marker of Nerve Injury. *Molecular and Cellular Neuroscience* **15**, 170–182 (2000). https://doi.org/10.1006/mcne.1999.0814

39 Chavan, S. S., Pavlov, V. A. & Tracey, K. J. Mechanisms and Therapeutic Relevance of Neuro-immune Communication. *Immunity* **46**, 927–942 (2017). https://doi.org/10.1016/j.immuni.2017.06.008

40 Bai, L. *et al.* Genetic Identification of Vagal Sensory Neurons That Control Feeding. *Cell* **179**, 1129–1143.e1123 (2019). https://doi.org/10.1016/j.cell.2019.10.031

41 Kupari, J., Häring, M., Agirre, E., Castelo-Branco, G. & Ernfors, P. An Atlas of Vagal Sensory Neurons and Their Molecular Specialization. *Cell Rep* **27**, 2508–2523.e2504 (2019). https://doi.org/10.1016/j.celrep.2019.04.096

42 Wang, Y. *et al.* Timing and Magnitude of Type I Interferon Responses by Distinct Sensors Impact CD8 T Cell Exhaustion and Chronic Viral Infection. *Cell Host & Microbe* **11**, 631–642 (2012). https://doi.org/10.1016/j.chom.2012.05.003

43 Wilson, E. B. *et al.* Blockade of chronic type I interferon signaling to control persistent LCMV infection. *Science* **340**, 202–207 (2013). https://doi.org/10.1126/science.1235208

44 Harker, J. A. *et al.* IL-6 and IL-27 play both distinct and redundant roles in regulating CD4 T-cell responses during chronic viral infection. *Front Immunol* **14**, 1221562 (2023). https://doi.org/10.3389/fimmu.2023.1221562

45 Cayrol, C. & Girard, J. P. Interleukin-33 (IL-33): A nuclear cytokine from the IL-1 family. *Immunol Rev* **281**, 154–168 (2018). https://doi.org/10.1111/imr.12619

46 Serve, S. & Löhning, M. Interleukin-33 and its receptor: multifaceted roles and emerging therapeutic potential. *Nature Reviews Immunology* (2026). https://doi.org/10.1038/s41577-026-01345-8

47 Giles, J. R. *et al.* Shared and distinct biological circuits in effector, memory and exhausted CD8(+) T cells revealed by temporal single-cell transcriptomics and epigenetics. *Nat Immunol* **23**, 1600–1613 (2022). https://doi.org/10.1038/s41590-022-01338-4

48 Hudson, W. H. *et al.* Proliferating Transitory T Cells with an Effector-like Transcriptional Signature Emerge from PD-1+ Stem-like CD8+ T Cells during Chronic Infection. *Immunity* **51**, 1043–1058.e1044 (2019). https://doi.org/10.1016/j.immuni.2019.11.002

49 Harty, J. T., Tvinnereim, A. R. & White, D. W. CD8+ T cell effector mechanisms in resistance

to infection. *Annu Rev Immunol* **18**, 275–308 (2000). https://doi.org/10.1146/annurev.immunol.18.1.275

50 Jordan, M. B., Hildeman, D., Kappler, J. & Marrack, P. An animal model of hemophagocytic lymphohistiocytosis (HLH): CD8+ T cells and interferon gamma are essential for the disorder. *Blood* **104**, 735–743 (2004). https://doi.org/10.1182/blood-2003-10-3413

51 Pachlopnik Schmid, J. *et al.* Neutralization of IFNgamma defeats haemophagocytosis in LCMV-infected perforin- and Rab27a-deficient mice. *EMBO Mol Med* **1**, 112–124 (2009). https://doi.org/10.1002/emmm.200900009

52 Redford, S. E., Varanasi, S. K., Sanchez, K. K., Thorup, N. R. & Ayres, J. S. CD4+ T cells regulate sickness-induced anorexia and fat wasting during a chronic parasitic infection. *Cell Rep* **42**, 112814 (2023). https://doi.org/10.1016/j.celrep.2023.112814

53 Hart, B. L. Biological basis of the behavior of sick animals. *Neurosci Biobehav Rev* **12**, 123–137 (1988). https://doi.org/10.1016/s0149-7634(88)80004-6

54 Pecchi, E., Dallaporta, M., Jean, A., Thirion, S. & Troadec, J. D. Prostaglandins and sickness behavior: old story, new insights. *Physiol Behav* **97**, 279–292 (2009). https://doi.org/10.1016/j.physbeh.2009.02.040

55 Liew, F. Y., Girard, J.-P. & Turnquist, H. R. Interleukin-33 in health and disease. *Nature Reviews Immunology* **16**, 676–689 (2016). https://doi.org/10.1038/nri.2016.95

56 Kim, J. V., Kang, S. S., Dustin, M. L. & McGavern, D. B. Myelomonocytic cell recruitment causes fatal CNS vascular injury during acute viral meningitis. *Nature* **457**, 191–195 (2009). https://doi.org/10.1038/nature07591

57 Feldman-Goriachnik, R., Belzer, V. & Hanani, M. Systemic inflammation activates satellite glial cells in the mouse nodose ganglion and alters their functions. *Glia* **63**, 2121–2132 (2015). https://doi.org/10.1002/glia.22881

58 Grill, H. J. & Hayes, M. R. The nucleus tractus solitarius: a portal for visceral afferent signal processing, energy status assessment and integration of their combined effects on food intake. *Int J Obes (Lond)* **33 Suppl 1**, S11–15 (2009). https://doi.org/10.1038/ijo.2009.10

59 Cheng, W. *et al.* Hindbrain circuits in the control of eating behaviour and energy balance. *Nat Metab* **4**, 826–835 (2022). https://doi.org/10.1038/s42255-022-00606-9

60 Florsheim, E. B. *et al.* Immune sensing of food allergens promotes avoidance behaviour. *Nature* **620**, 643–650 (2023). https://doi.org/10.1038/s41586-023-06362-4

61 Touhara, K. K. *et al.* Parasites trigger epithelial cell crosstalk to drive gut-brain signalling. *Nature* **653**, 465–473 (2026). https://doi.org/10.1038/s41586-026-10281-5

62 Jindal, J., Hill, J., Harte, J., Dunachie, S. J. & Kronsteiner, B. Starvation and infection: The role of sickness-associated anorexia in metabolic adaptation during acute infection. *Metabolism* **161**, 156035 (2024). https://doi.org/10.1016/j.metabol.2024.156035

63 Kazane, K. R. *et al.* Metabolomic profiling reveals the potential of fatty acids as regulators of exhausted CD8 T cells during chronic viral infection. *Proc Natl Acad Sci U S A* **123**, e2419820122 (2026). https://doi.org/10.1073/pnas.2419820122

Figures and figure legends:

Figure 1

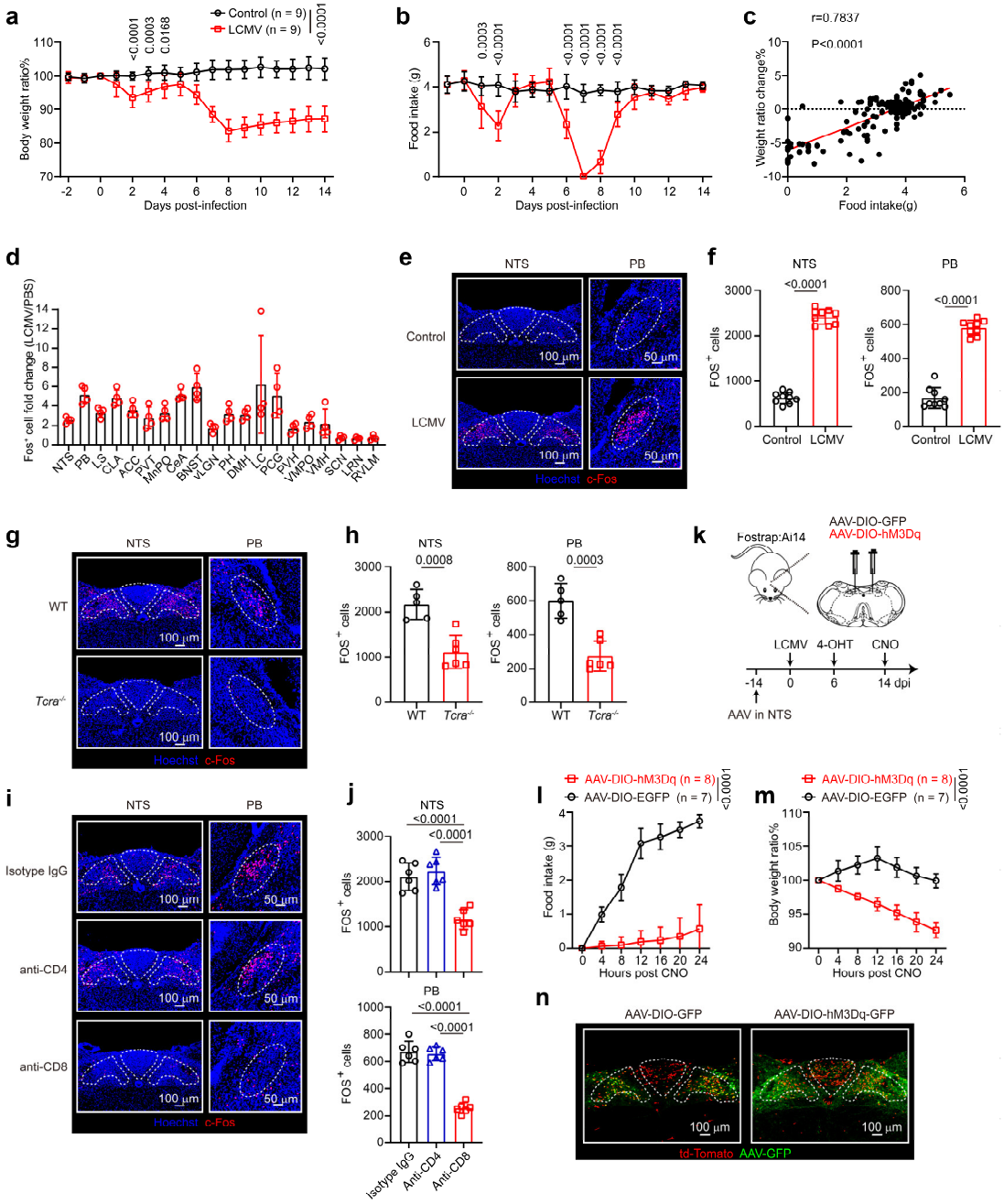


Figure 1. Virus-specific CD8⁺ T cells engage an NTS-PB circuit to drive late-phase anorexia during LCMV infection.

a, b, Body weight (**a**) and daily food intake (**b**) of control and LCMV-infected wild-type mice. **c,** Correlation between daily food intake and body weight change during LCMV infection. **d,** Quantification of c-Fos induction in the indicated brain regions during the peak anorexic phase of LCMV infection, expressed as fold change relative to control mice. **e, f,** Representative immunofluorescence images of c-Fos expression in the NTS and PB (**e**) and quantification of c-Fos⁺ cells (**f**) in control and LCMV-infected mice. **g, h,** Representative immunofluorescence images (**g**) and quantification of c-Fos⁺ cells (**h**) in the NTS and PB of LCMV-infected wild-type and *Tcra*$^{-/-}$ mice. **i, j,** Representative immunofluorescence

images (**i**) and quantification of c-Fos$^+$ cells (**j**) in the NTS and PB of LCMV-infected wild-type mice treated with an isotype control, anti-CD4, or anti-CD8 antibody. **k,** Schematic of the experimental strategy for activity-dependent labeling and chemogenetic reactivation of NTS neurons activated during LCMV infection in FosTRAP;Ai14 mice. **l, m,** Food intake (**l**) and body weight (**m**) following CNO-mediated reactivation of infection-tagged NTS neurons expressing hM3Dq or control GFP. **n,** Representative fluorescence images showing tdTomato-labeled infection-activated NTS neurons and AAV-GFP expression in mice injected with AAV-DIO-GFP or AAV-DIO-hM3Dq-GFP. Data are pooled from two (**d, g, h, i, j, l, m** and **n**) or three (**a, b, c, e** and **f**) independent experiments. Graphs show mean ± SD. Statistical significance was determined by two-way ANOVA (**a, l** and **m**), two-way ANOVA with multiple-comparisons correction (**b**), two-tailed unpaired Student's t test (**f** and **h**), one-way ANOVA with multiple-comparisons correction (**j**), and Pearson correlation with two-sided *P* value (**c**). The overall *P* value indicates the interaction (**a, l** and **m**). Scale bars are indicated in the images.

Figure 2

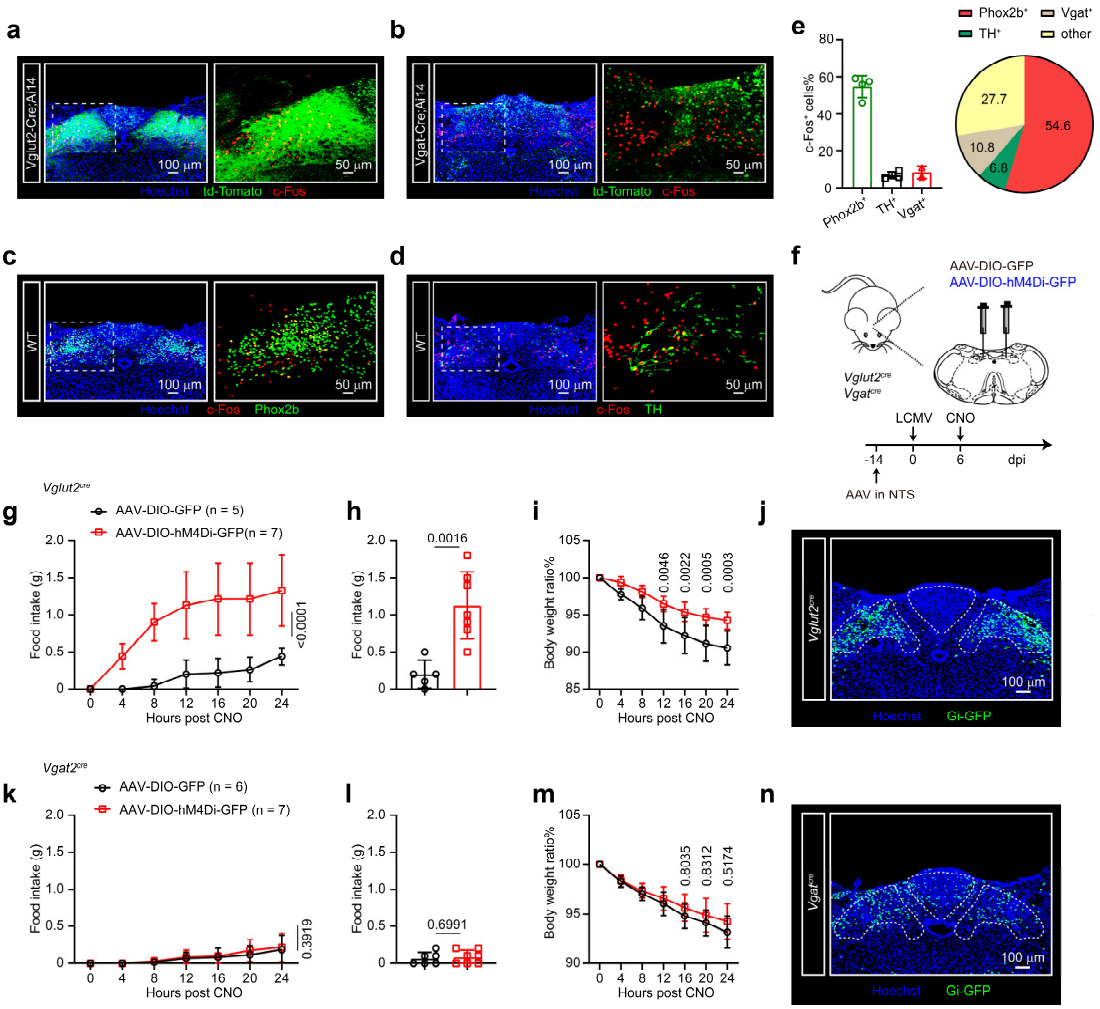


Figure 2. Excitatory Vglut2$^+$ neurons in the NTS are required for LCMV-induced late phase anorexia.

a, b, Representative immunofluorescence images of c-Fos expression in genetically labeled Vglut2$^+$ (**a**)

or Vgat^{+} (**b**) neurons in the NTS during the late anorexic phase of LCMV infection. **c, d,** Representative immunofluorescence images of c-Fos expression in Phox2b^{+} (**c**) or TH^{+} (**d**) neurons in the NTS. **e,** Quantification of the proportions of c-Fos^{+} NTS neurons expressing Phox2b, TH, or Vgat, and the relative composition of the infection-activated NTS neuronal population. **f,** Schematic of the experimental strategy for chemogenetic inhibition of Vglut2^{+} or Vgat^{+} NTS neurons during LCMV infection. **g-i,** Cumulative food intake following CNO administration (**g**), total food intake over 12 h (**h**), and body weight trajectories (**i**) in LCMV-infected Vglut2-Cre mice expressing GFP or hM4Di in the NTS. **j,** Representative fluorescence image showing AAV-mediated GFP expression in the NTS of Vglut2-Cre mice. **k-m,** Cumulative food intake following CNO administration (**k**), total food intake over 12 h (**l**), and body weight trajectories (**m**) in LCMV-infected Vgat-Cre mice expressing GFP or hM4Di in the NTS. **n,** Representative fluorescence image showing AAV-mediated GFP expression in the NTS of Vgat-Cre mice. Data are pooled from two independent experiments. Graphs show mean ± SD. Statistical significance was determined by two-way ANOVA (**g** and **k**), two-way ANOVA with multiple-comparisons correction (**i** and **m**), two-tailed unpaired Student's t test (**h** and **l**). The overall *P* value indicates the interaction (**g** and **k**). Scale bars are indicated in the images.

Figure 3

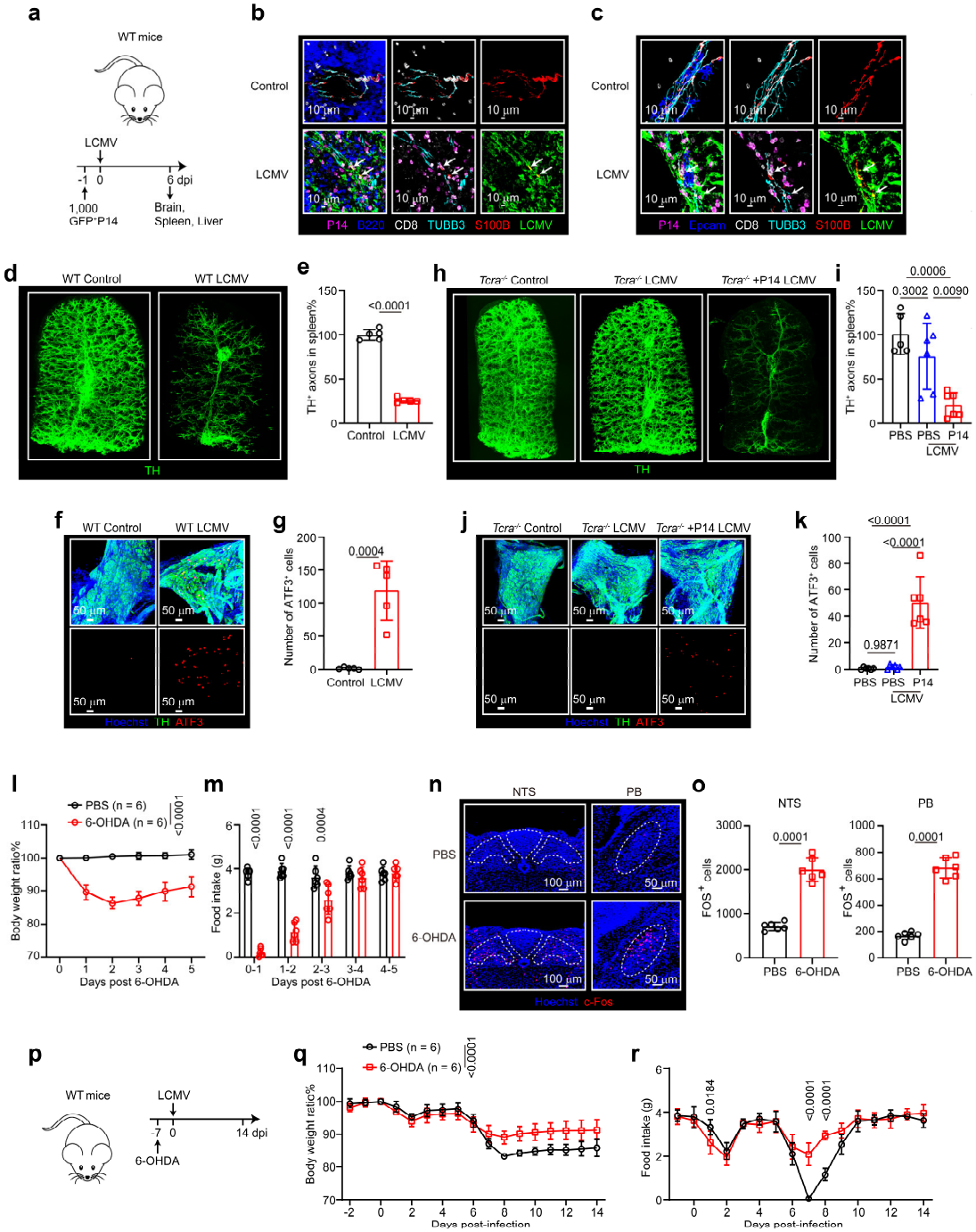


Figure 3. Virus-specific CD8⁺ T cells induce sympathetic nerve injury to drive infection-associated anorexia.

a, Schematic of the experimental strategy for assessing the tissue distribution of antigen-specific CD8⁺ T cells during LCMV infection. **b, c,** Representative immunofluorescence images showing the spatial distribution of transferred GFP⁺ P14 CD8⁺ T cells, LCMV antigen, and neural structures in the spleen (**b**) and liver (**c**) of control and LCMV-infected mice. B220 and EpCAM were used to delineate splenic and hepatic tissue compartments, respectively, whereas TUBB3 and S100B were used to visualize peripheral neural and glial elements. **d, e,** Representative three-dimensional images of TH⁺ sympathetic innervation

(**d**) and quantification of TH$^+$ axons (**e**) in the spleen of control and LCMV-infected wild-type mice. **f, g,** Representative immunofluorescence images of ATF3 expression in the celiac ganglion (CG) (**f**) and quantification of ATF3$^+$ cells (**g**) in control and LCMV-infected mice. **h, i,** Representative images of splenic TH$^+$ sympathetic innervation (**h**) and quantification of TH$^+$ axons (**i**) in the spleen of uninfected *Tcra*$^{-/-}$ mice, LCMV-infected *Tcra*$^{-/-}$ mice with or without adoptive transfer of P14 CD8$^+$ T cells. **j, k,** Representative immunofluorescence images of ATF3 expression in CG (**j**) and quantification of ATF3$^+$ cells (**k**) in uninfected *Tcra*$^{-/-}$ mice, LCMV-infected *Tcra*$^{-/-}$ mice with or without transfer of P14 CD8$^+$ T cells. **l, m,** Body weight trajectories (**l**) and daily food intake (**m**) of wild-type mice treated with PBS or 6-hydroxydopamine (6-OHDA). **n, o,** Representative immunofluorescence images of c-Fos expression (**n**) and quantification of c-Fos$^+$ cells (**o**) in the NTS and PB following PBS or 6-OHDA treatment. **p,** Schematic of the experimental strategy for chemical sympathectomy before LCMV infection. **q, r,** Body weight trajectories (**q**) and daily food intake (**r**) in PBS- or 6-OHDA-pretreated mice following LCMV infection. Data are pooled from two independent experiments. Graphs show mean ± SD. Statistical significance was determined by two-way ANOVA (**l** and **q**), two-way ANOVA with multiple-comparisons correction (**m** and **r**), one-way ANOVA with multiple-comparisons correction (**i** and **k**), two-tailed unpaired Student's t test (**e, g** and **o**). The overall *P* value indicates the interaction (**l** and **q**). Scale bars are indicated in the images.

Figure 4

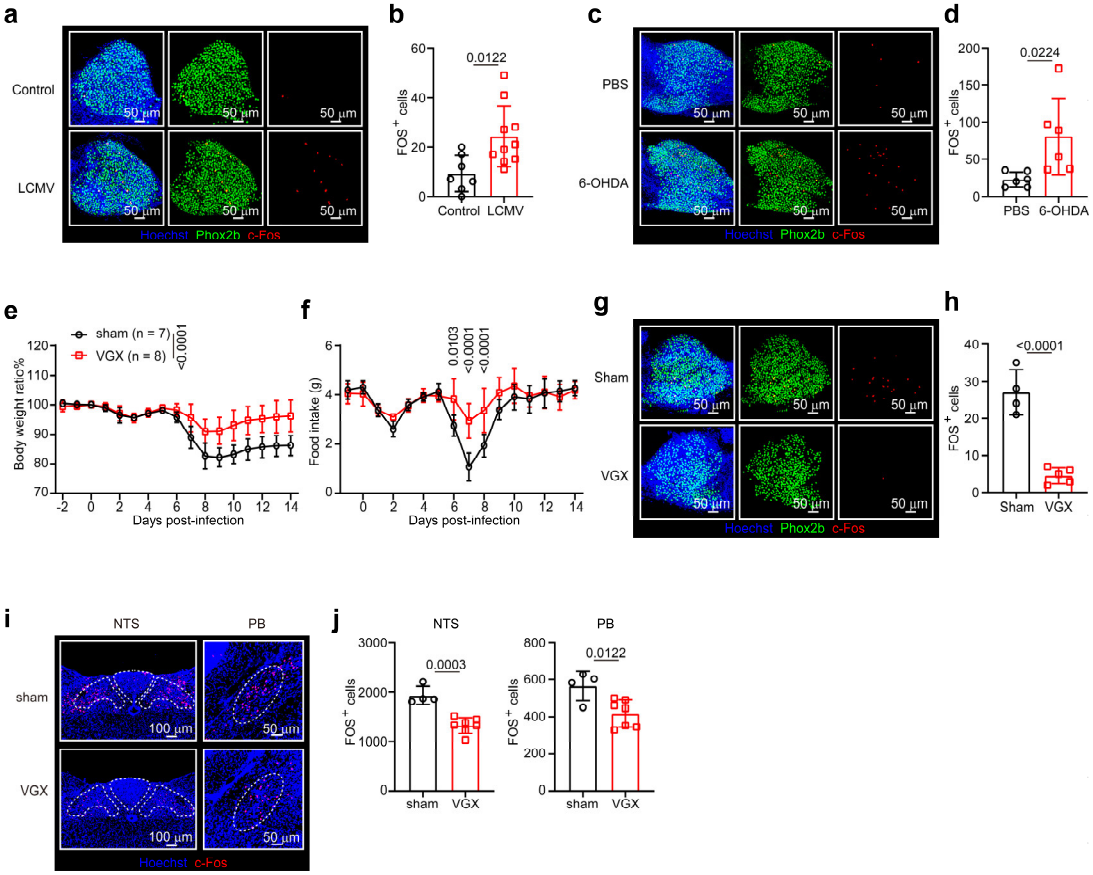


Figure 4. Vagal afferents relay peripheral signals to the NTS.

a, b, Representative immunofluorescence images of c-Fos expression (**a**) and quantification of c-Fos$^+$ cells (**b**) in Phox2b$^+$ neurons in the nodose ganglion (NG) of control and LCMV-infected mice. **c, d,** Representative immunofluorescence images of c-Fos expression (**c**) and quantification of c-Fos$^+$ cells (**d**) in Phox2b$^+$ NG neurons of PBS and 6-OHDA-treated mice. **e, f,** Body weight trajectories (**e**) and daily food intake (**f**) in sham-operated and bilaterally subdiaphragmatic vagotomized (VGX) mice following LCMV infection. **g, h,** Representative immunofluorescence images of c-Fos expression (**g**) and quantification of c-Fos$^+$ cells (**h**) in Phox2b$^+$ NG neurons of sham-operated and VGX mice following LCMV infection. **i, j,** Representative immunofluorescence images of c-Fos expression (**i**) and quantification of c-Fos$^+$ cells (**j**) in the NTS and PB of sham-operated and VGX mice following LCMV infection. Data are pooled from two independent experiments. Graphs show mean ± SD. Statistical significance was determined by two-way ANOVA (**e**), two-way ANOVA with multiple-comparisons correction (**f**), two-tailed unpaired Student's t test (**b, d, h** and **j**). The overall *P* value indicates the interaction (**e**). Scale bars are indicated in the images.

Figure 5

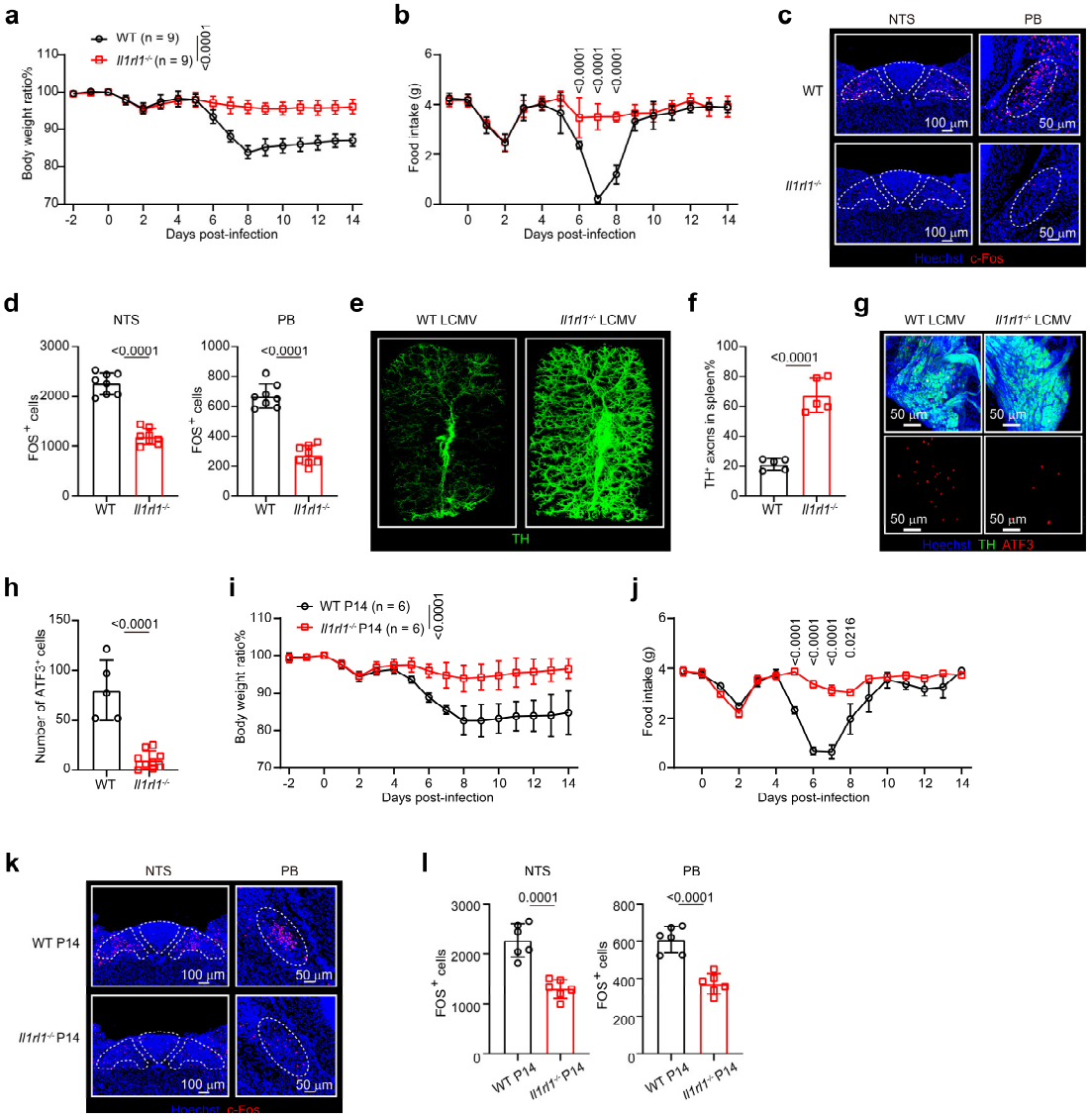


Figure 5. CD8⁺ T cell-intrinsic ST2-MyD88 signaling drives late-phase anorexia and engages the anorexia-associated neural circuit.

a, b, Body weight trajectories (**a**) and daily food intake (**b**) of wild-type and *Il1rl1*$^{-/-}$ mice following LCMV infection. **c, d,** Representative immunofluorescence images of c-Fos expression (**c**) and quantification of c-Fos^{+} cells (**d**) in the NTS and PB of LCMV-infected wild-type and *Il1rl1*$^{-/-}$ mice. **e, f,** Representative three-dimensional images of TH^{+} sympathetic innervation (**e**) and quantification of TH^{+} axons (**f**) in the spleen of LCMV-infected wild-type and *Il1rl1*$^{-/-}$ mice. **g, h,** Representative immunofluorescence images of ATF3 expression (**g**) and quantification of ATF3^{+} cells (**h**) in the CG of LCMV-infected wild-type and *Il1rl1*$^{-/-}$ mice. **i, j,** Body weight trajectories (**i**) and daily food intake (**j**) of LCMV-infected *Il1rl1*$^{-/-}$ recipient mice that were transferred with wild-type or *Il1rl1*$^{-/-}$ P14 CD8^{+} T cells. **k, l,** Representative immunofluorescence images of c-Fos expression (**k**) and quantification of c-Fos^{+} cells (**l**) in the NTS and PB of *Il1rl1*$^{-/-}$ recipients reconstituted with wild-type or *Il1rl1*$^{-/-}$ P14 CD8^{+} T cells. Data are pooled from two (**c, d, e, f, g, h, i, j, k** and **l**) or three (**a** and **b**) independent experiments.

Statistical significance was determined by two-way ANOVA (**a** and **i**), two-way ANOVA with multiple-comparisons correction (**b** and **j**), two-tailed unpaired Student's t test (**d, f, h** and **l**). The overall *P* value indicates the interaction (**a** and **i**). Scale bars are indicated in the images.

Figure 6

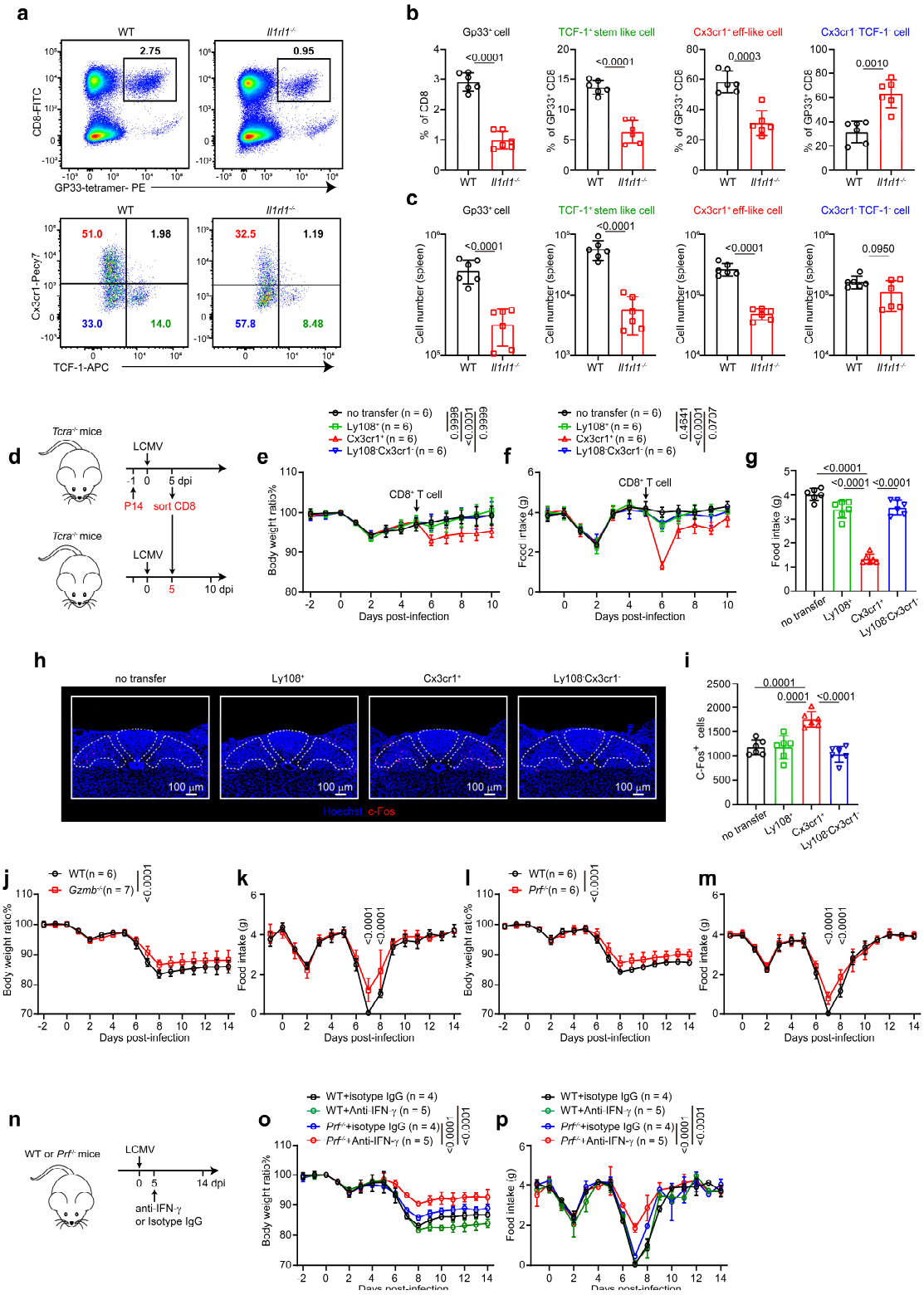
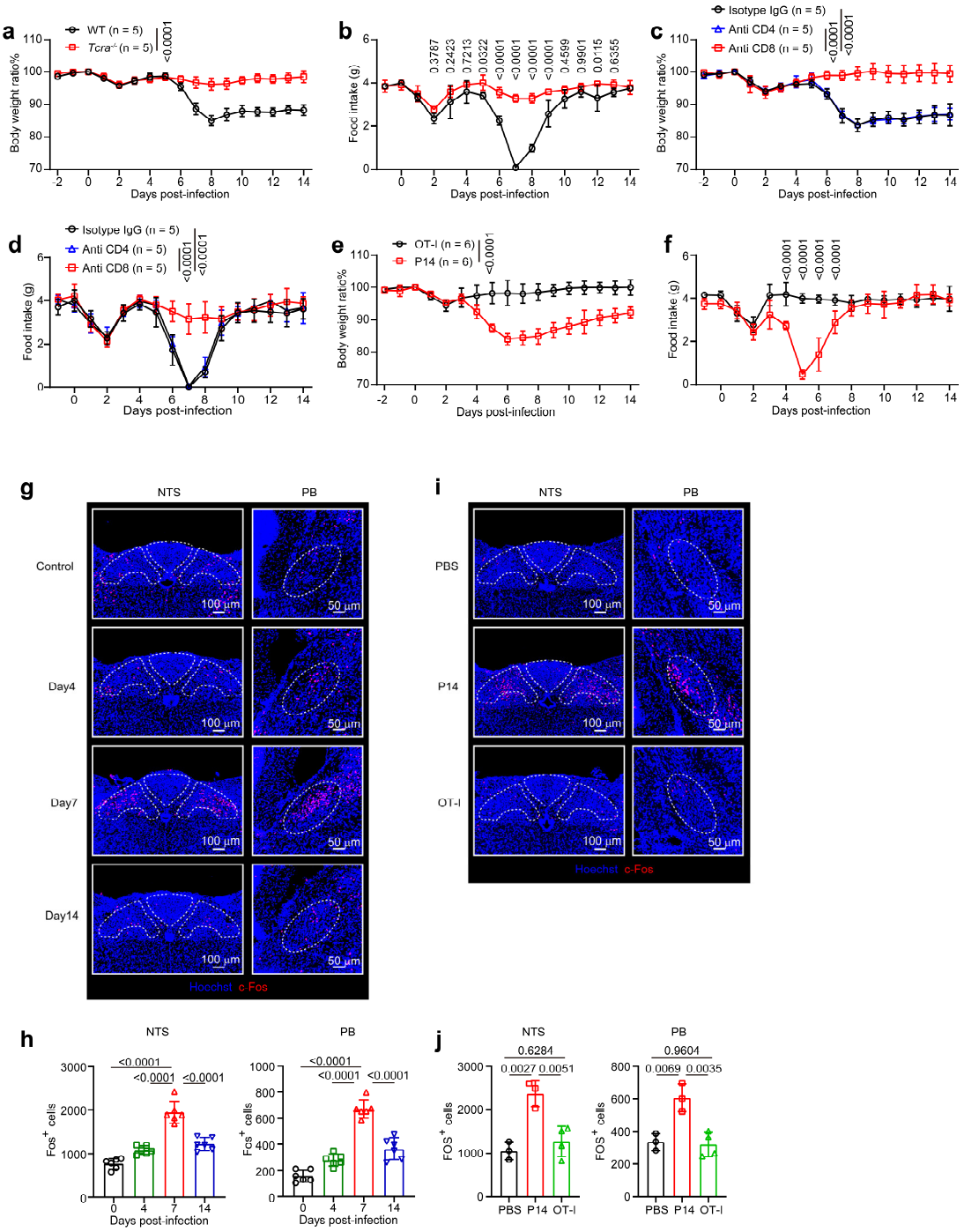


Figure 6. Effector programs of antiviral CD8$^+$ T cells drive infection-associated anorexia.

a, Representative flow cytometry plots showing splenic GP33-specific CD8$^+$ T cells and the distribution of TCF-1$^+$ and CX3CR1$^+$ subpopulations in LCMV-infected wild-type and *Il1rl1*$^{-/-}$ mice. **b, c,** Frequencies (**b**) and absolute numbers (**c**) of GP33-specific CD8$^+$ T cells, TCF-1$^+$ stem-like cells, CX3CR1$^+$ effector-like cells, and CX3CR1$^-$TCF-1$^-$ cells in the spleen of LCMV-infected wild-type and *Il1rl1*$^{-/-}$ mice. **d,** Schematic of the experimental strategy for adoptive transfer of distinct virus-specific CD8$^+$ T-cell subpopulations into LCMV infection-matched *Tcra*$^{-/-}$ recipient mice. **e-g,** Body weight trajectories (**e**), daily food intake (**f**), and cumulative food intake over 24h (**g**) in recipient mice that received no cells, Ly108$^+$, CX3CR1$^+$, or Ly108$^-$CX3CR1$^-$ P14 cells. **h, i,** Representative immunofluorescence images of c-Fos expression (**h**) and quantification of c-Fos$^+$ cells (**i**) in the NTS of indicated recipient mice. **j-m,** Body weight trajectories (**j** and **l**) and daily food intake (**k** and **m**) in LCMV-infected wild-type and *Gzmb*$^{-/-}$ mice (**j** and **k**) or *Prf1*$^{-/-}$ mice (**l** and **m**). **n,** Schematic of the experimental strategy for IFN-γ neutralization during LCMV infection. **o, p,** Body weight trajectories (**o**) and daily food intake (**p**) in infected wild-type and *Prf1*$^{-/-}$ mice treated with an IFN-γ-neutralizing antibody or an isotype control antibody. Data are pooled from two independent experiments. Graphs show mean ± SD. Statistical significance was determined by two-way ANOVA (**j** and **l**), two-way ANOVA with multiple-comparisons correction (**e, f, k, m, o** and **p**), one-way ANOVA with multiple-comparisons correction (**g** and **i**), two-tailed unpaired Student's t test (**b, c**). The overall *P* value indicates the interaction (**j** and **l**). Scale bars are indicated in the images.

Extended Data Figure 1

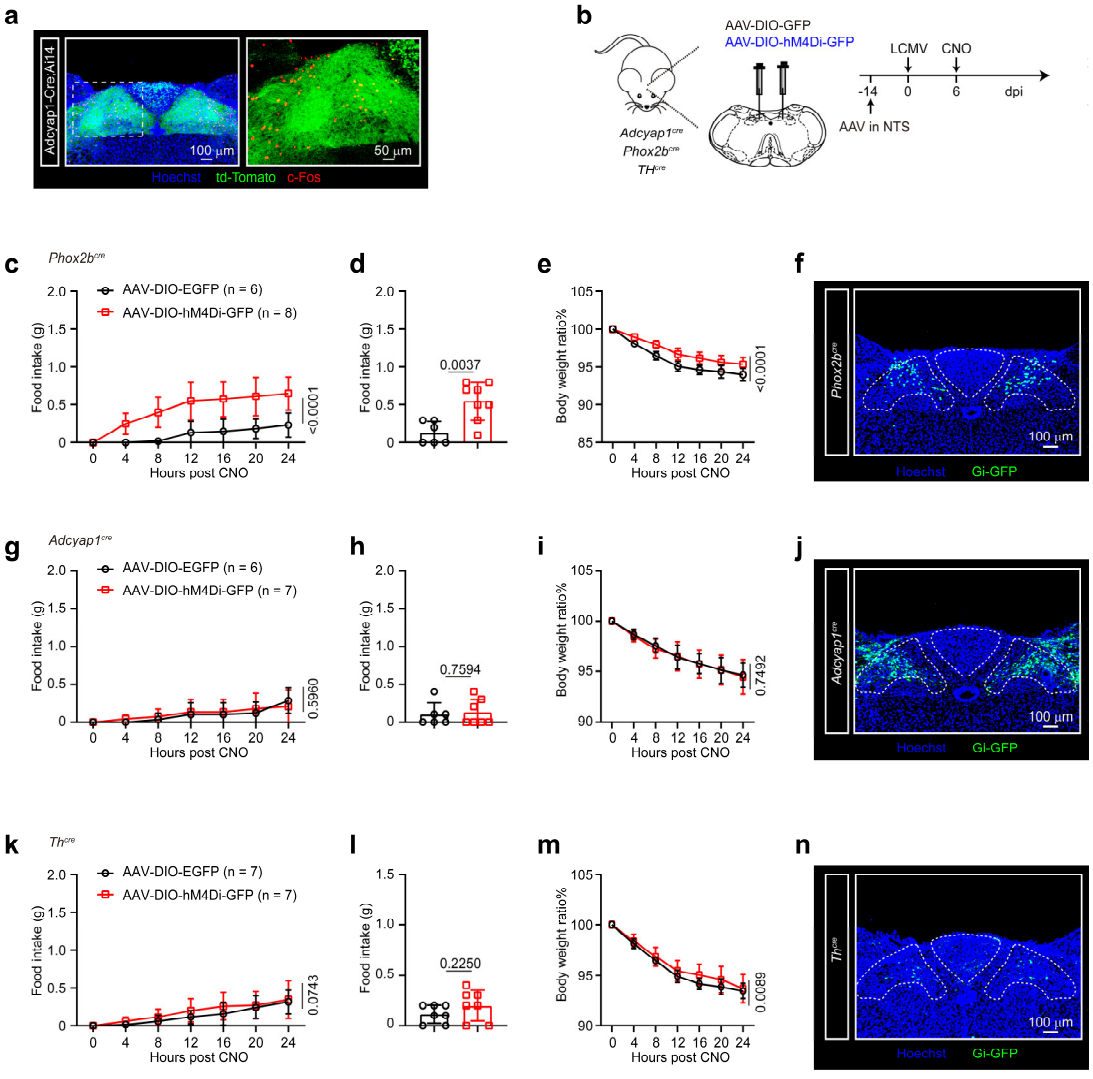


Extended Data Figure 1. Antigen-specific CD8⁺ T cells are required for late-phase anorexia and NTS-PB activation during LCMV infection.

a, b, Body weight trajectories (**a**) and daily food intake (**b**) of wild-type and *Tcra*$^{-/-}$ mice following LCMV infection. **c, d,** Body weight trajectories (**c**) and daily food intake (**d**) of LCMV-infected wild-type mice treated with an isotype control antibody, an anti-CD4 or an anti-CD8 antibody. **e, f,** Body weight trajectories (**e**) and daily food intake (**f**) of LCMV-infected *Tcra*$^{-/-}$ mice reconstituted with LCMV-specific P14 or antigen-irrelevant OT-I CD8⁺ T cells. **g, h,** Representative immunofluorescence images showing

c-Fos expression (**g**) and quantification of c-Fos$^+$ cells (**h**) in the NTS and PB at the indicated time points following LCMV infection. **i, j,** Representative immunofluorescence images of c-Fos expression (**i**) and quantification of c-Fos$^+$ cells (**j**) in the NTS and PB of LCMV-infected *Tcra*$^{-/-}$ mice receiving PBS, P14, or OT-I T cells. Data are pooled from two independent experiments. Graphs show mean ± SD. Statistical significance was determined by two-way ANOVA (**a** and **e**), two-way ANOVA with multiple-comparisons correction (**b, c, d** and **f**), one-way ANOVA with multiple-comparisons correction (**h** and **j**). The overall *P* value indicates the interaction (**a** and **e**). Scale bars are indicated in the images.

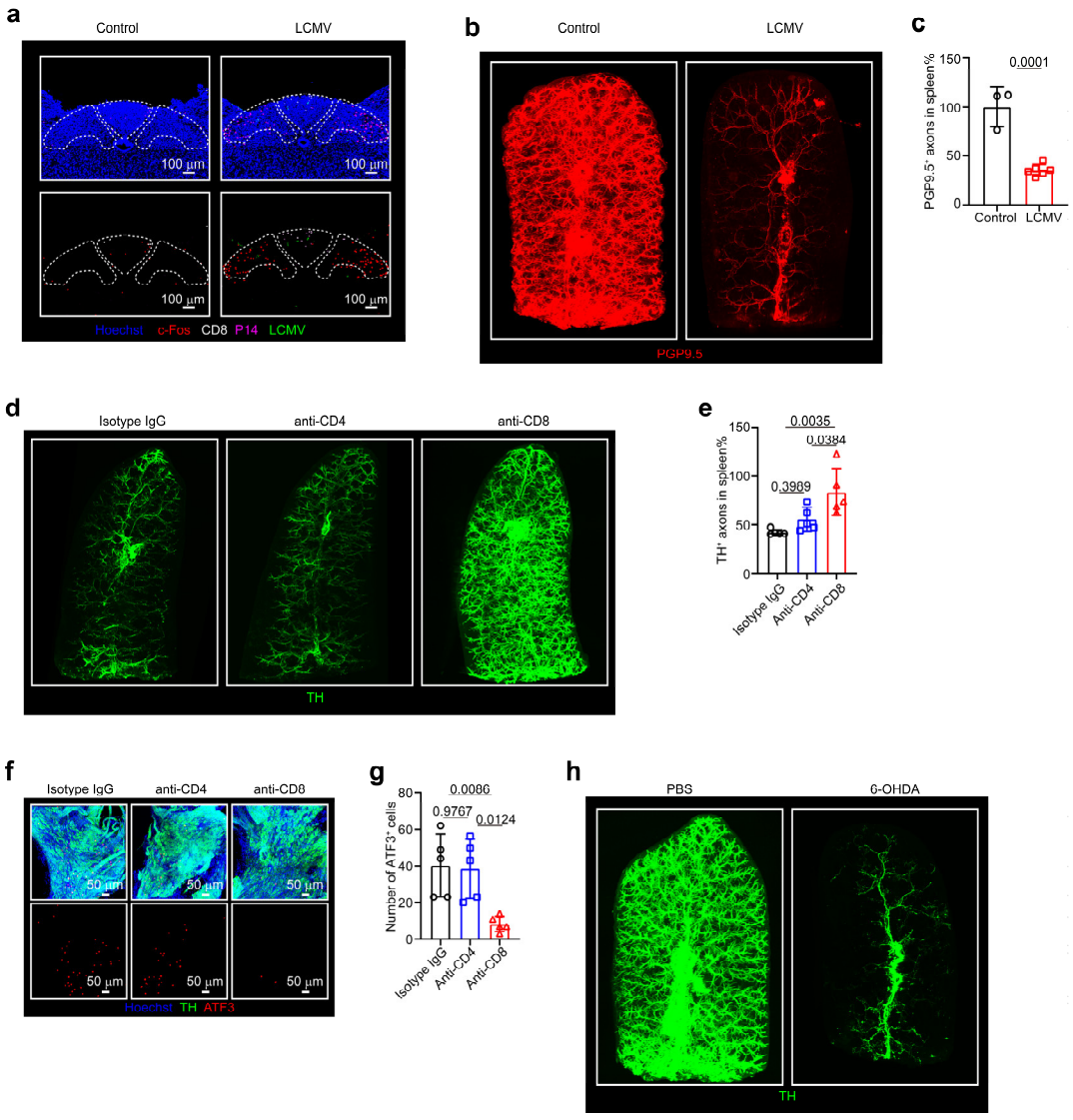
Extended Data Figure 2



Extended Data Figure 2. Phox2b$^+$ NTS neurons contribute to LCMV-induced anorexia.
a, Representative immunofluorescence images showing c-Fos expression in genetically labeled Adcyap1$^+$ NTS neurons during the peak anorexic phase of LCMV infection. **b,** Schematic of the experimental strategy for chemogenetic inhibition of Phox2b$^+$, Adcyap1$^+$, or TH$^+$ NTS neurons. **c-e,** Cumulative food intake following CNO administration (**c**), total food intake over 12 h (**d**), and body

weight trajectories (**e**) in LCMV-infected Phox2b-Cre mice expressing GFP or hM4Di in the NTS. **f,** Representative fluorescence image showing AAV-mediated GFP expression in the NTS of Phox2b-Cre mice. **g-i,** Cumulative food intake following CNO administration (**g**), total food intake over 12 h (**h**), and body weight trajectories (**i**) in LCMV-infected Adcyap1-Cre mice expressing GFP or hM4Di in the NTS. **j,** Representative fluorescence image showing AAV-mediated GFP expression in the NTS of Adcyap1-Cre mice. **k-m,** Cumulative food intake following CNO administration (**k**), total food intake over 12 h (**l**), and body weight trajectories (**m**) in LCMV-infected Th-Cre mice expressing GFP or hM4Di in the NTS. **n,** Representative fluorescence image showing AAV-mediated GFP expression in the NTS of Th-Cre mice. Data are pooled from two (**c, d, e, f, g, h, i** and **j**) or three (**k, l, m** and **n**) independent experiments. Graphs show mean ± SD. Statistical significance was determined by two-way ANOVA (**c, g** and **k**), two-way ANOVA with multiple-comparisons correction (**e, i** and **m**), two-tailed unpaired Student's t test (**d, h** and **l**). The overall *P* value indicates the interaction (**c, g** and **k**). Scale bars are indicated in the images.

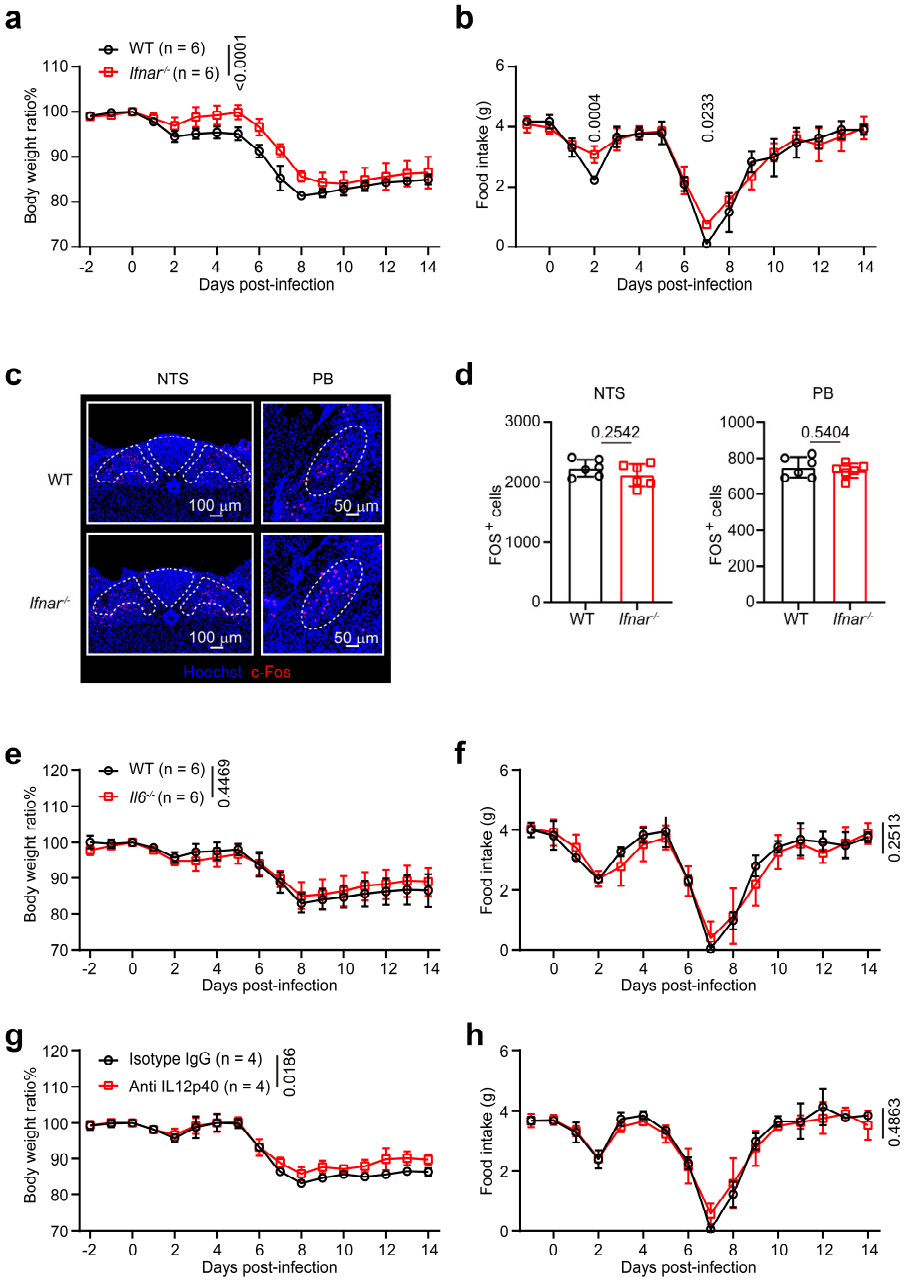
Extended Data Figure 3



Extended Data Figure 3. Antiviral CD8$^+$ T-cell response induces sympathetic denervation of the spleen.

a, Representative immunofluorescence images showing the spatial distribution of transferred GFP$^+$ P14 CD8$^+$ T cells, LCMV antigen and c-Fos$^+$ cells in the brainstem of control and LCMV-infected mice during the late anorexic phase. **b, c,** Representative three-dimensional images of PGP9.5$^+$ nerve fibers in the spleen (**b**) and quantification of PGP9.5$^+$ axons (**c**) in control and LCMV-infected mice. **d, e,** Representative three-dimensional images of TH$^+$ sympathetic innervation (**d**) and quantification of TH$^+$ axons (**e**) in the spleen of LCMV-infected wild-type mice treated with control IgG, anti-CD4 or anti-CD8. **f, g,** Representative immunofluorescence images of ATF3 expression in the celiac ganglion (CG) (**f**) and quantification of ATF3$^+$ cells (**g**) in LCMV-infected wild-type mice treated with control IgG, anti-CD4 or anti-CD8. **h,** Representative three-dimensional images of TH$^+$ sympathetic innervation in the spleen of mice treated with PBS or 6-OHDA. Data are from single experiment (**a**) or pooled from two independent experiments (**b-h**). Graphs show mean ± SD. Statistical significance was determined by two-tailed unpaired Student's t test (**c**), one-way ANOVA with multiple-comparisons correction (**e** and **g**). Scale bars are indicated in the images.

Extended Data Figure 4

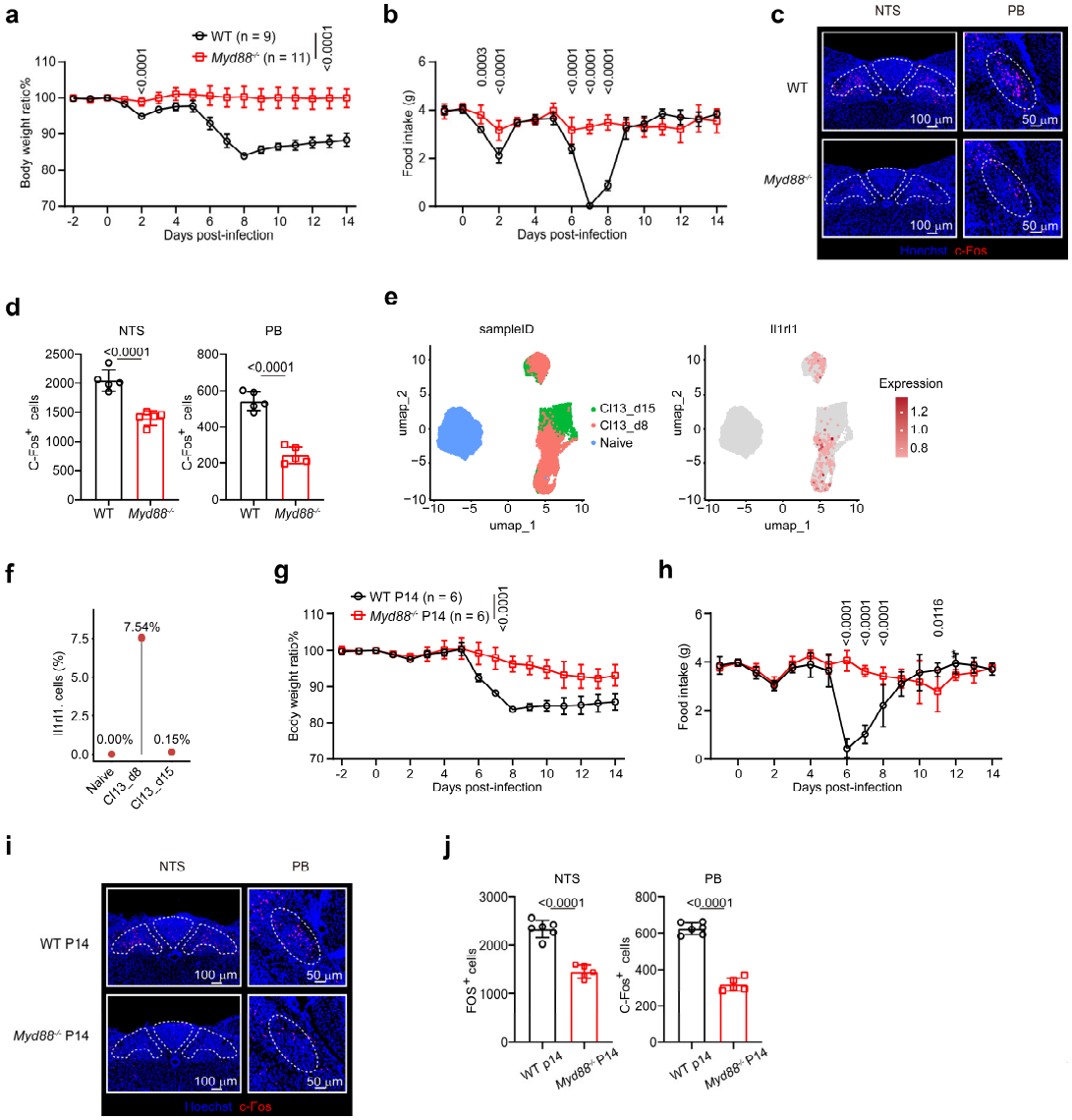


Extended Data Figure 4. Type I interferon, IL-6, and IL-12/23 signaling are dispensable for late-phase LCMV-induced anorexia.

a, b, Body weight trajectories (**a**) and daily food intake (**b**) of wild-type and *Ifnar*$^{-/-}$ mice following LCMV infection. **c, d,** Representative immunofluorescence images showing c-Fos expression (**c**) and quantification of c-Fos^{+} cells (**d**) in the NTS and PB of LCMV-infected wild-type and *Ifnar*$^{-/-}$ mice. **e, f,** Body weight trajectories (**e**) and daily food intake (**f**) of LCMV-infected wild-type and *Il6*$^{-/-}$ mice. **g, h,** Body weight trajectories (**g**) and daily food intake (**h**) of LCMV-infected mice treated with an isotype control antibody or an anti-IL-12p40 antibody. Data are pooled from two independent experiments. Graphs show mean ± SD. Statistical significance was determined by two-way ANOVA (**a, e, g, f** and

h), two-way ANOVA with multiple-comparisons correction (**b**), two-tailed unpaired Student's t test (**d**). The overall *P* value indicates the interaction (**a, e, g, f** and **h**). Scale bars are indicated in the images.

Extended Data Figure 5

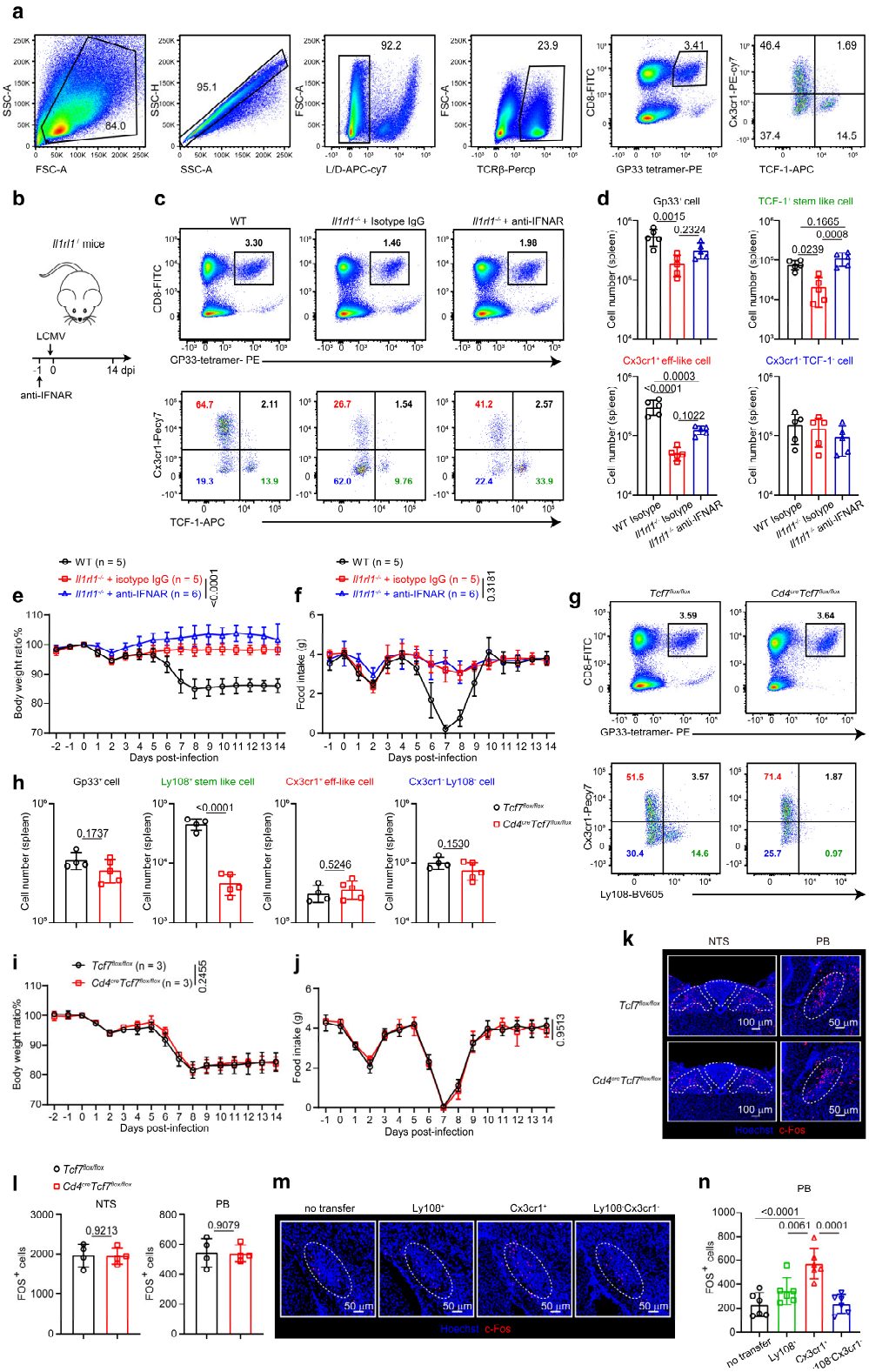


Extended Data Figure 5. MyD88 is required for both early- and late-phase anorexia.

a, b, Body weight trajectories (**a**) and daily food intake (**b**) of wild-type and *Myd88*$^{-/-}$ mice following LCMV infection. **c, d,** Representative immunofluorescence images showing c-Fos expression (**c**) and quantification of c-Fos^{+} cells (**d**) in the NTS and PB of LCMV-infected wild-type and *Myd88*$^{-/-}$ mice. **e, f,** UMAP visualization of CD8^{+} T-cell populations at the indicated stages of LCMV infection (**e**) and *Il1rl1* expression across these populations (**f**), based on single-cell RNA-sequencing data from Giles et al. (2022). **g, h,** Body weight trajectories (**g**) and daily food intake (**h**) of *Myd88*$^{-/-}$ recipient mice receiving wild-type or *Myd88*$^{-/-}$ P14 CD8^{+} T cells one day before LCMV infection. **i, j,** Representative immunofluorescence images showing c-Fos expression (**i**) and quantification of c-Fos^{+} cells (**j**) in the NTS and PB of *Myd88*$^{-/-}$ recipients reconstituted with wild-type or *Myd88*$^{-/-}$ P14 cells. Data are pooled

from two (**c, d, g, h, i,** and **j**) or three (**a** and **b**) independent experiments. Graphs show mean ± SD. Statistical significance was determined by two-way ANOVA (**a** and **g**), two-way ANOVA with multiple-comparisons correction (**b** and **h**), two-tailed unpaired Student's t test (**d** and **j**). The overall *P* value indicates the interaction (**a** and **g**). Scale bars are indicated in the images.

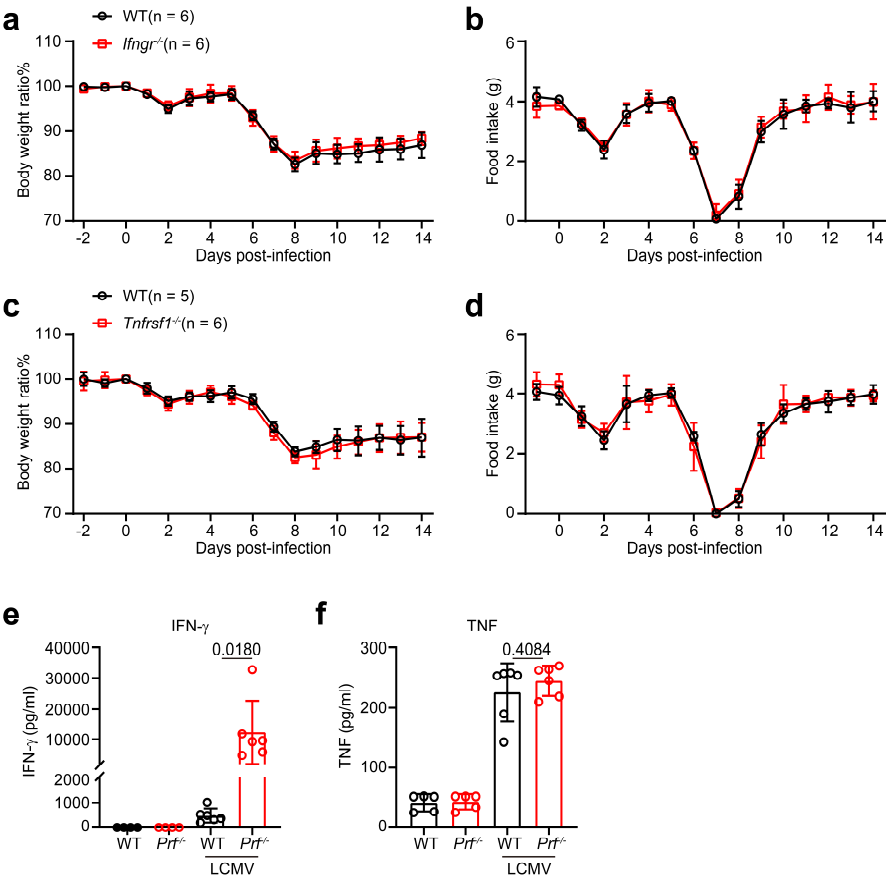
Extended Data Figure 6



Extended Data Figure 6. TCF-1$^+$ stem-like CD8$^+$ T cells are dispensable for adaptive immunity-mediated anorexia.

a, Representative flow cytometry plots showing the gating strategy used to identify GP33-specific CD8$^+$ T cells and their TCF-1- and CX3CR1-defined subsets during LCMV infection. **b,** Schematic of the experimental strategy for blocking type I IFN receptor signaling in *Il1rl1*$^{-/-}$ mice during LCMV infection. **c,** Representative flow cytometry plots showing GP33-specific CD8$^+$ T cells and the distribution of TCF-1$^+$ and CX3CR1$^+$ subsets in LCMV-infected wild-type mice and *Il1rl1*$^{-/-}$ mice treated with an isotype control or an anti-IFNAR antibody. **d,** Absolute numbers of GP33-specific CD8$^+$ T cells, TCF-1$^+$ stem-like cells, CX3CR1$^+$ effector-like cells, and CX3CR1$^-$TCF-1$^-$ cells in the spleen of the indicated groups. **e, f,** Body weight trajectories (**e**) and daily food intake (**f**) of LCMV-infected wild-type mice and *Il1rl1*$^{-/-}$ mice treated with an isotype control or an anti-IFNAR antibody. **g,** Representative flow cytometry plots showing GP33-specific CD8$^+$ T cells and the distribution of TCF-1$^+$ and CX3CR1$^+$ subsets in LCMV-infected *Tcf7*$^{fl/fl}$ and Cd4-Cre *Tcf7*$^{fl/fl}$ mice. **h,** Absolute numbers of GP33-specific CD8$^+$ T cells, Ly108$^+$ stem-like cells, CX3CR1$^+$ effector-like cells, and CX3CR1$^-$TCF-1$^-$ cells in the spleen of the indicated groups. **i, j,** Body weight trajectories (**i**) and daily food intake (**j**) of LCMV-infected *Tcf7*$^{fl/fl}$ and Cd4-Cre *Tcf7*$^{fl/fl}$ mice. **k, l,** Representative immunofluorescence images showing c-Fos expression (**k**) and quantification of c-Fos$^+$ cells (**l**) in the NTS and PB of LCMV-infected *Tcf7*$^{fl/fl}$ and Cd4-Cre *Tcf7*$^{fl/fl}$ mice. **m, n,** Representative immunofluorescence images showing c-Fos expression (**m**) and quantification of c-Fos$^+$ cells (**n**) in the PB of infection-matched *Tcra*$^{-/-}$ recipients receiving no cells or Ly108$^+$, CX3CR1$^+$ or Ly108$^-$CX3CR1$^-$ P14 cells. Data are from single experiment (**g-l**) or pooled from two independent experiments (**c-f, m-n**). Graphs show mean ± SD. Statistical significance was determined by two-way ANOVA (**i** and **j**), two-way ANOVA with multiple-comparisons correction (**e** and **f**), one-way ANOVA with multiple-comparisons correction (**d** and **n**), two-tailed unpaired Student's t test (**h, l**). The overall *P* value indicates the interaction (**i** and **j**). Scale bars are indicated in the images.

Extended Data Figure 7



Extended Data Figure 7. Physiological IFN-γ and TNF signaling are dispensable for LCMV-induced anorexia.

a, b, Body weight trajectories (**a**) and daily food intake (**b**) of wild-type and *Ifngr*$^{-/-}$ mice following LCMV infection. **c, d,** Body weight trajectories (**c**) and daily food intake (**d**) of wild-type and *Tnfrsf1*$^{-/-}$ mice following LCMV infection. **e, f,** Serum concentrations of IFN-γ (**e**) and TNF (**f**) in uninfected and LCMV-infected wild-type and *Prf1*$^{-/-}$ mice. Data are pooled from two independent experiments. Graphs show mean ± SD. Statistical significance was determined by two-way ANOVA (**a, b, c** and **d**), two-tailed unpaired Student's t test (**e** and **f**).

Supplementary Video 1. Three-dimensional visualization of whole-brain c-Fos expression following LCMV infection.

Representative three-dimensional reconstruction of the whole brain from a wild-type (WT) mouse at day 6 after LCMV clone 13 infection. The brain was subjected to tissue clearing and whole-mount immunostaining for c-Fos (red), enabling visualization of the spatial distribution of c-Fos^{+} cells throughout the brain.

Supplementary Video 2. Three-dimensional visualization of splenic sympathetic innervation following LCMV infection.

Representative three-dimensional reconstruction of the spleen from a wild-type (WT) mouse at day 6 after LCMV clone 13 infection. Tyrosine hydroxylase (TH) immunostaining (green) labels sympathetic nerve fibers, enabling visualization of the three-dimensional organization and distribution of TH^+ sympathetic innervation throughout the spleen. Related to Fig. 3d, e.

Materials and Methods

Mice

C57BL/6 (JAX: # 000664), *Fos*$^{2A\text{-}iCreER}$ (TRAP2) (JAX: #030323), Ai14 (JAX: #007914), *Phox2b*^{cre} (JAX: #016223), *Ifngr1*$^{-/-}$ (JAX: #003288), *Ifnar1*$^{-/-}$ (JAX: #028288), *Tcra*$^{-/-}$ (JAX: #002116), *Il6*$^{-/-}$ (JAX: #002650), *Prf1*$^{-/-}$ (JAX: #002407), *Vglut2*^{cre} (JAX: #016963), *Cd4*^{cre} (JAX: #017336), *Vgat*^{cre} (JAX: #028862), OVA257-264-specific T cell transgenic OT-I (JAX: #003831), *Adcyap1*^{cre} (JAX: #030155), P14 TCRVα2Vβ8 (JAX: #037394) mouse strains were derived from The Jackson Laboratory (JAX), *Gzmb*$^{-/-}$ mice were purchased from GemPharmatech (T015670); *Tnfrsf1a*$^{-/-}$ (JAX: #002818) and *Myd88*$^{-/-}$ mice were kindly provided by Dr. Jiahuai Han (Xiamen University)[64,65], *Th*^{cre} (JAX: #008601) mice were kindly provided by Dr. Ren Xu (Xiamen University)[66], *Il1rl1*$^{-/-}$ mice were kindly provided by Dr. Hong Zhou (Anhui Medical University)[67], *Tcf7*^{flox} mice were kindly provided by Dr. Lilin Ye (Army Medical University)[68]. All mouse lines were bred and maintained under specific pathogen-free condition at the Laboratory Animal Center of Xiamen University with a 12h light/dark cycle (lights on from 8 a.m. to 8 p.m.), a controlled temperature of 22℃-24℃, and humidity of 50–70%. Unless stated otherwise, both male and female mice were used for experiments. All animal experiments were approved by the Animal Care and Use Committee of Xiamen University (XMULAC20210072).

METHOD DETAILS

Body weight and food intake measurement

Age- and sex-matched littermates were individually housed and acclimated until baseline body weight and food intake were stable. Mice had ad libitum access to food and water throughout the experimental period. Body weight and food intake were measured daily at 8:00 a.m. Daily food intake was calculated as the difference in food weight between consecutive measurements. Body weight was expressed as a percentage of baseline body weight, defined as the body weight measured on the day of treatment or infection (100%).

LCMV infection

8-12 weeks old mice were infected with 2×10^6 PFU LCMV clone 13 intravenously.

LCMV Cl13 virus was grown in BHK-21 cells (ATCC, CCL-10), for viral titration, Vero cells (ATCC, CCL-81) were trypsinized, resuspended, and seeded into 96-well plates at 2×10^4 cells per well. Ten-fold serial dilutions of the virus stock were prepared in a 96-well plate using a multichannel pipette. Briefly, 15 μL of the undiluted virus stock was added to the first well and serially diluted 10-fold to the desired dilution, typically up to 10^{-6}. After incubation for 20 h at 37°C in a humidified atmosphere containing 5% CO_2, the culture medium was removed. Cells

were washed with PBS and fixed with 30 μL of 4% paraformaldehyde (PFA) per well for 30 min. During fixation, blocking buffer (PBS add 3% BSA and 0.3% Triton X-100 supplemented with 1% goat serum) and primary antibody staining buffer (PBS add 3% BSA and 0.3% Triton X-100 supplemented with 1% goat serum) with anti-LCMV (VL4, BioXcell, # BE0106) were prepared. After removal of the fixative, cells were blocked with 30 μL of blocking buffer for 30 min, followed by incubation with 30 μL of primary antibody staining solution at 4°C for 48 h. Cells were then washed twice with PBS and incubated with secondary antibody staining solution containing goat anti-rat Alexa Fluor 488 antibody (Thermo Fisher Scientific, #A-11006) for 2–3 h. Fluorescent foci were counted under a fluorescence microscope, and the viral titer was calculated accordingly.

Antibodies and pharmacological treatments

For depletion of $CD4^+$ or $CD8^+$ T cells, 250 μg of anti-CD4 (Bioxcell, #BE0003-1), anti-CD8 (Bioxcell, #BE0061) or isotype control antibody (BioXcell, # BE0089) was administered intraperitoneally to mice at 1 day before and 4 days after LCMV infection.

For in vivo blockade of IL-12/23 signaling, 250 μg of anti-IL-12 p40 (C17.8, Bio X Cell, #BP0051) or isotype control antibody (BioXcell, # BE0089) was administered intraperitoneally to mice on the day of LCMV infection and on day 3 post infection.

For in vivo blockade of IFNAR, *Il1rl1*$^{-/-}$ mice received an intraperitoneal injection of 1 mg of anti-IFNAR antibody (MAR1-5A3, Selleck, #A2121) or isotype control IgG (BioXcell, # BE0089) one day before LCMV infection.

To neutralize IFN-γ in vivo, WT or *prf1*$^{-/-}$ mice were intraperitoneally injected with 300 μg of anti-IFN-γ (Selleck, #A2152) or isotype control antibody (BioXcell, # BE0089) on day 5 post LCMV infection.

For chemical sympathetic denervation, 8-12-week old mice were treated intraperitoneally with 6-hydroxydopamine hydrobromide (6-OHDA; MedChemExpress, #HY-B1081A; 150 mg/kg) for two consecutive days, freshly prepared in PBS containing 0.2% ascorbic acid. Control mice received the corresponding vehicle. For experiments assessing the acute effects of sympathetic denervation on feeding behavior, body weight and food intake were monitored following 6-OHDA administration. In separate experiments, tissues were harvested 24 h after 6-OHDA treatment for subsequent analysis. For experiments investigating the effects of pre-existing sympathetic denervation on LCMV-induced anorexia, mice were allowed to recover for one week following 6-OHDA treatment before LCMV infection.

Preparation of cell suspensions, antibody staining and flow cytometry

To isolate $CD8^+$ T cells from the spleen, spleens were harvested and mechanically dissociated in ice-cold phosphate-buffered saline (PBS) supplemented with 2% fetal bovine serum (FBS) and 0.5 mM EDTA (Sigma-Aldrich, Cat. No. 2085657). The dissociated splenic tissue was passed through a 70-μm cell strainer to obtain single-cell suspensions. Following red blood cell lysis, the cells were stained with the fixable viability dye Zombie Red or eFluor™ 780 Fixable Viability Dye (Invitrogen) for 30 min at 4°C. Fc receptors were subsequently blocked with anti-CD16/32 antibody (clone 2.4G2; BD Biosciences) for 15 min at 4°C. Cell surface proteins were stained for 30 min at 4°C with the following antibodies: anti-CD8 (53-6.7), anti-TCRβ (H57-597), anti-PD-1 (29F.1A12), anti-CD366/TIM-3 (RMT3-23), anti-CX3CR1 (SA011F11) all

from BioLegend, anti-Ly-108 (13G3) from BD optibuild, H2Db GP33 SA-PE Tetramer from NIH. Nuclear proteins were stained overnight at 4 °C after permeabilization and fixation (eBioscience, Cat#: 88-8115-40) using anti-TCF1/TCF7 (C63D9) from Cell Signaling Technology. The cell counts were normalized to a predetermined number of counting beads (BioLegend, Cat#: 424902). Cells were analyzed using a CytoFLEX LX (Beckman Coulter), LSRFortessa, or LSRFortessa X-20 (BD Biosciences) flow cytometer. Data were analyzed using FlowJo software (version 10.5.3).

Isolation and adoptive transfer of P14/OT-I cells

P14/OT-I mice were euthanized by cervical dislocation, and peripheral lymph nodes and spleens were harvested and mechanically dissociated in ice-cold PBS supplemented with 2% fetal bovine serum (FBS) and 0.5 mM EDTA. Following red blood cell lysis, single-cell suspensions were passed through a 40-μm cell strainer. $CD8^+$ T cells were subsequently enriched by negative selection using streptavidin-conjugated magnetic beads. The biotinylated antibody cocktail contained antibodies against CD4, CD11b, CD11c, B220, Ly-6G/Ly-6C, F4/80, Ter119, and TCRγ/δ. Following magnetic depletion of non-$CD8^+$ cells, the enriched 2×10^5 $CD8^+$ T cells were collected and adoptively transferred into *Tcra*$^{-/-}$ mice via tail-vein injection.

In selected experiments, 1×10^4 P14, *Il1rl1*$^{-/-}$ P14, or *Myd88*$^{-/-}$ P14 cells were purified using the same protocol and adoptively transferred via tail vein injection into *Il1rl1*$^{-/-}$ or *Myd88*$^{-/-}$ recipient mice one day prior to LCMV infection.

In distinct antigen-specific $CD8^+$ T-cell subsets transfer to infected match mice experiment, 2×10^5 P14 cells were purified and transfer to *Tcra*$^{-/-}$ mice one day prior to LCMV infection, on day 5 post infection, spleens were harvested and mechanically dissociated in ice-cold PBS supplemented with 2% FBS and 2 mM EDTA. The resulting single-cell suspensions were passed through a 40-μm cell strainer. Following antibody staining, Cx3cr1$^+$ $CD8^+$, Ly108$^+$ $CD8^+$ and Cx3cr1$^-$Ly108$^-$ $CD8^+$ T cell populations were separately purified by fluorescence-activated cell sorting (FACS) using a BD FACSAria III cell sorter. Then 1×10^6 Ly108$^+$ $CD8^+$ T cells, 3×10^6 Cx3cr1$^+$ $CD8^+$ or Cx3cr1$^-$Ly108$^-$ $CD8^+$ T cells were adoptively transferred into infected matched *Tcra*$^{-/-}$ mice, respectively.

ELISA

Blood samples were collected and allowed to stand at room temperature for 30 minutes. Samples were centrifuged at 800 × g for 15 min at 4°C, and the resulting serum supernatants were carefully transferred to fresh tubes and stored at −80°C until further use.

Serum IFN-γ and TNF levels were determined using enzyme-linked immunosorbent assay (ELISA) kits (TNF: R&D system, #DY410; IFN-γ: R&D system, #DY485) following the manufacturer's recommended protocol. In brief, 96-well strip plates were coated with 1 μg/mL capture antibody diluted in PBS and incubated overnight at 4°C. The wells were subsequently blocked with 5 mg/mL bovine serum albumin (BSA) in PBS for 2 h at room temperature. After three washes with PBST (PBS containing 0.05% Tween-20), 100 μL of each sample was added to the wells and incubated for 2 h at room temperature. The wells were washed again three times with PBST, followed by incubation with 1 μg/mL biotinylated detection antibody diluted in PBS containing 5 mg/mL BSA for 2–3 h at room temperature. Then plates were washed and

incubated with streptavidin-conjugated horseradish peroxidase (streptavidin-HRP). After a final wash step, 100 µL of substrate solution was added, and the plate was incubated in the dark at room temperature to allow color development. The enzymatic reaction was terminated by adding 50 µL of stop solution, and the optical density was read at 450 nm using a microplate reader.

Immunofluorescence staining

Mice from each treatment group were deeply anesthetized with 2.5% Avertin and subsequently transcardially perfused with 0.9% saline, followed by 4% paraformaldehyde (PFA). The brain, celiac ganglion and nodose ganglion were then harvested and post-fixed in 4% PFA overnight at 4°C. For liver and spleen, mice were perfused with PBS alone, and the collected tissues were fixed overnight at 4°C in BD Cytofix/Cytoperm solution (BD Bioscience, #554722). All tissues except the celiac and nodose ganglion were cryoprotected in 30% sucrose prior to sectioning. Samples were embedded in O.C.T. compound (Sakura Finetek, #4583) and sectioned at -20°C using a cryostat (Leica, CM1950). Sectioning parameters varied according to tissue type: brain sections were prepared at 40 µm thickness, whereas liver and spleen sections were cut at 30 µm. The celiac and nodose ganglia were processed as whole-mount preparations without sectioning. Brain sections were rinsed twice with PBS and then incubated in blocking buffer composed of PBS containing 3% BSA, 1% normal mouse serum, 1% normal donkey serum, and 0.3% Triton X-100. Primary antibody incubation was carried out using unconjugated antibodies overnight at 4°C, followed by exposure to fluorophore-conjugated secondary antibodies for 2-3 h at room temperature in a humidified dark chamber. Between each staining step, sections were rinsed three to five times with 1× PBS for 5 min each.

The celiac and nodose ganglia were processed according to the procedure described above, except that incubations with primary and secondary antibodies were prolonged to 48 h and 24 h, respectively. Washes between staining steps consisted of five rinses with PBS (10 min each).

Sections of liver and spleen were rehydrated with 1x PBS, then blocked in 1 x PBS containing 1% normal mouse serum, 1% normal goat serum, 1% bovine serum albumin, and 0.2% Triton X-100. Staining was performed as described for brain sections, except that fluorophore-conjugated primary antibodies were incubated for 24 hours at room temperature in a dark humidified chamber.

After staining, slides were mounted with Fluormount G (Southern Biotech, #0100-01). Images were acquired on a Leica TCS SP8 and Leica STELLARIS 8 STED confocal microscope or an automated slider scanner (Zeiss AxioScan7). Images were analyzed with Imaris software (Bitplane) or ZEN (Zeiss). All antibodies were diluted in relevant blocking buffer, and the following antibodies were used: rabbit anti-c-Fos (9F6, Cell Signaling Technology, #2250), goat anti-Phox2b (polyclonal goat IgG, R&D Systems, #AF4940), chicken anti-Tyrosine hydroxylase (Sigma-Aldrich, #AB9702), rat anti-LCMV nucleoprotein (VL4, Bioxcell, #BE0106), rabbit anti-β3-tubulin (D71G9, Cell Signaling Technology, #5568S), rabbit anti-S100B (EP1576Y，Abcam, #ab52642), Alexa Fluor 647 anti-mouse CD8a Antibody (53-6.7, Biolegend, #100724), BV480 rat anti-mouse CD8a Antibody (53-6.7, BD, # 566096), eFluor™ 450 B220 Antibody (RA3-6B2, eBioscience, #48-0452-82), eFluor™ 450 CD326 (EpCAM) Antibody (G8.8, eBioscience, # 48-5791-82), goat anti-rabbit Alexa Fluor 647 (Thermo Fisher

Scientific, #A-21244), goat anti-rabbit Alexa Fluor 594 (Thermo Fisher Scientific, #A-11012), goat anti-rat Alexa Fluor 555 (Thermo Fisher Scientific, #A-21434), donkey anti-rabbit Alexa Fluor 647 (Thermo Fisher Scientific, #A-31573), donkey anti-goat Alexa Fluor 555 (Thermo Fisher Scientific, #A-21432), donkey anti-chicken Alexa Fluor 647 (Thermo Fisher Scientific, #A-78952), donkey anti-rabbit Alexa Fluor 488 (Thermo Fisher Scientific, #A-21206), donkey anti-rabbit Alexa Fluor 555 (Thermo Fisher Scientific, #A-31572) and donkey anti-goat Alexa Fluor 647 (Thermo Fisher Scientific, #A-21447).

TRAP2 labelling for chemogenetics

Bilateral stereotaxic injections of 250 nL of AAV2/9-hSyn-DIO-hM3D(Gq)-eGFP-WPRE-pA (Taitool, #S0260-9) or the control vector AAV2/9-hSyn-DIO-mGFP-WPRE-pA (Taitool, #S0276-9) (2×10^{12} V.G/mL) were performed into the NTS of TRAP: Ai14 mice at 8 weeks of age. After a 2-week surgical recovery, animals were challenged with LCMV. On day 6 post infection, 4-OHT (50 mg/kg, MedChemExpress, #HY-16950A) was administered to induce DREADDs expression. An additional week later, CNO (1 mg/kg, Sigma-Aldrich, #C0832) was injected intraperitoneally at 20:00 to evaluate its effects on body weight and food intake. To confirm viral transduction, coronal brain sections between bregma -7.2 and -8.2 mm were obtained at 40-μm intervals and stained for tdTomato and GFP by immunohistochemistry.

Chemogenetic inhibition of NTS neurons

For chemogenetic inhibition experiments, the inhibitory DREADD virus AAV2/9-hSyn-DIO-hM4D(Gi)-eGFP-WPRE-Pa (Taitool, #S0286-9) or the control virus AAV2/9-hSyn-DIO-EGFP-WPRE-pA (Taitool, #S0746-9) was stereotaxically injected into the NTS of *Vglut2*^{cre}, *Vgat*^{cre}, *Th*^{cre}, *Adcyap1*^{cre}, and *Phox2b*^{cre} mice as described as TRAP2 labelling for chemogenetics to achieve cell type-specific inhibition or control manipulation. Following a 2-week recovery period, mice were infected with LCMV at 8:00 AM. At 20:00 on day 6 post infection, CNO (1 mg/kg) was intraperitoneally administered to suppress DREADD-expressing neuronal activity, and food intake was monitored over the subsequent 24 h. After body weight and food intake measurements, coronal brain sections spanning from bregma -7.2 mm to -8.2 mm were collected for immunofluorescent staining of GFP to verify viral expression.

Subdiaphragmatic vagotomy

For Subdiaphragmatic vagotomy, 6-8 weeks old mice were deeply anesthetized with 2.5% Avertin. Following shaving and disinfection of the abdominal surface with 75% ethanol, a midline incision was made to expose the peritoneal cavity. Under a stereomicroscope, the anterior and posterior vagal nerve trunks were localized along the distal esophagus, gently dissected free from adjacent connective tissue, and a 2-3 mm segment was excised from each branch to preclude reinnervation. In sham-operated controls, the nerves were visualized but left intact. The abdominal wall and skin were subsequently closed with sutures. Animals were allowed to recover for a minimum of 2 weeks before experimental procedures. Vagotomy efficacy was verified by gastric emptying assessment; successful denervation was confirmed by the observation of pronounced gastric distension at necropsy, indicative of substantial impairment in gastric emptying.

Whole-tissue clearing

Immunolabeling-enabled three-dimensional imaging of solvent-cleared organs (iDISCO) of mouse brain and spleen was performed as previously described[69]. Briefly, mice were infected with LCMV. On day 6 post infection, mice were anesthetized, and then intracardial perfusion with 1×PBS containing 20 μg/ml heparin (Sigma, H3393-50KU), followed by freshly prepared 4% PFA. Brain and spleen were carefully dissected, post-fixed in 4% PFA for 24 hours at 4 °C, then washed 3 times with 1×PBS (1 hour per wash). Subsequently, tissues were dehydrated through a graded methanol series (20%, 40%, 60%, 80% and 100% methanol in ddH2O), each step lasts for 2 hours at room temperature. The tissues were then incubated at 4℃ for 48h with the mixture of 30% H_2O_2 and 100% methanol (1:10). After that, tissues were rehydrated through a reverse methanol gradient (80%, 60%, 40%, 20% methanol in ddH2O), and 1×PBS, each step lasted for 2 h at room temperature. Finally, tissues were incubated in PTx.2 (1×PBS /0.2% Triton X-100/10% DMSO) at 37℃ overnight.

For tissue permeabilization, spleens were incubated in permeabilization buffer (1x PBS/0.2% Triton X-100/ 20% DMSO/ 0.3M glycine) at 37℃ for 2 days (brains for 4 days), then blocked in blocking buffer (PTx.2+3% normal donkey serum) at 37℃ for 1 day (brains for 3 days). For immunostaining, spleens were incubated with primary antibody, which was prepared in PTwH (1×PBS /0.2% Tween-20/10 μg/ml heparin) / 3% normal donkey serum at 37℃ for 3 days (brains for 5 days). Following primary incubation, spleens were washed extensively with PTwH, and exchanged every 8 hours for 2 days (brains for 4 days), then incubated with secondary antibody prepared in the same antibody dilution buffer at 37℃ for 3 days (brains for 5 days). Spleens were finally washed with PTwH for 2 days before clearing (brains for 4 days), with fresh buffer exchanged every 8h. All steps were performed with gentle shaking. The primary antibody used was rabbit anti-c-Fos (9F6, Cell Signaling Technology, #2250; 1:1,000), rabbit anti-TH (1:1,000, Sigma, #AB152), rabbit anti-PGP9.5 (1:1000, Proteintech, #14730-1 AP) and followed by a secondary donkey anti-rabbit Alexa Fluor 647 antibody (1:500, Thermo Fisher Scientific, #A-31573).

For optical clearing, tissues were re-dehydrated through a graded methanol series as mentioned above. Spleens were incubated twice with 66% dichloromethane (DCM; DCM: methanol=2:1), each for 2.5 hours in room temperature with shaking (brains for 4 h). Samples were subsequently treated with 100% DCM (Sigma-Aldrich, #270997-2L) for 1 hour, and repeated three times. Finally, samples were incubated in dibenzyl ether (DBE, Sigma-Aldrich, #108014-1KG) for refractive index matching without shaking, and stored at room temperature in the dark until imaging. Images were captured using a light-sheet microscope (NuoHai LS18, China) equipped with a 4×objective lens.

Quantification and Statistical analysis

Quantification of c-Fos$^+$ neurons in the NTS and PB. Brains were serially sectioned into 40-μm-thick coronal sections. Every third section containing the nucleus of the solitary tract (NTS) and the parabrachial nucleus (PB) was systematically sampled throughout the rostrocaudal extent of each region. c-Fos$^+$ cells were counted in each sampled section, and the counts were summed and multiplied by 3 to estimate the total number of c-Fos$^+$ cells in each region. For statistical analysis, each mouse was considered an independent biological replicate, with the estimated total cell count for each region used as the corresponding measurement.

For quantification of TH^+/PGP9.5+ nerve fiber volume fraction in cleared spleen, three-dimensional volumetric quantification was performed with Imaris software (Bitplane, version 10.0.0). The Imaris Surface tool was applied to the TH/PGP9.5 channel to generate a three-dimensional surface object representing the nerve fiber. Segmentation thresholds were set based on fluorescence intensity. The total imaged spleen volume was obtained directly from the Volume rendering object in Imaris without additional segmentation.

Statistical analyses were performed using GraphPad Prism (version 8). Data are presented as mean ± SD, as indicated in the figure legends. Comparisons between two independent groups were performed using two-tailed unpaired Student's t-tests. Comparisons among multiple groups were performed using one-way ANOVA followed by appropriate multiple-comparisons tests. Longitudinal measurements of body weight and food intake were analyzed using two-way repeated-measures ANOVA, with group and time as factors. The group × time interaction was used to assess differences in temporal response profiles. For comparisons between groups at individual time points, post hoc multiple-comparisons tests were performed following two-way ANOVA. Adjusted P values from these comparisons are indicated where applicable. $P < 0.05$ was considered statistically significant.

Data availability

All data supporting the findings of this study are available within the paper and its Supplementary Information files. Source data are provided with this paper. Additional data are available from the corresponding author upon reasonable request.

Acknowledgments

We thank Dr. Jiahuai Han (Xiamen University) for *Tnfrsf1a*$^{-/-}$ and *Myd88*$^{-/-}$ mice, Dr. Ren Xu (Xiamen University) for *Th*^{cre} mice, Dr. Hong Zhou (Anhui Medical University) for *Il1rl1*$^{-/-}$ mice, Dr. Lilin Ye (Army Medical University) for *Tcf7*^{flox} mice, Qingfeng Liu and Xiufeng Sun in Core facility of biomedical sciences of Xiamen University for confocal and flow cytometry technical support, Jianfeng Wu, Xiuqing Zheng and Suqin Wu in Laboratory Animal Center of Xiamen University for experimental animal management and in vitro fertilization service. This work was supported by the National Natural Science Foundation of China (32270953 and 22521102 to K.M., 82603445 to S.Y.), the Natural Science Foundation of Fujian Province of China (2025J011006 to K.M.), the Scientific Research Foundation of the State Key Laboratory of Vaccines for Infectious Diseases, Xiang'an Biomedicine Laboratory (2023XAKJ0101036 to K.M.), the Fundamental Research Funds for the Central Universities (20720260015 to K.M.), the China Postdoctoral Science Foundation (2026M792893 to S.Y.), and the Postdoctoral Fellowship Program of China Postdoctoral Science Foundation (GZB20250646 to S.Y.).

Author contributions

K.M. conceived this study, generated hypotheses. C.L., S.Y., and Y.S. performed most of the experiments and analyzed the data. X.L. and Y.S. assisted with subdiaphragmatic vagotomy and stereotaxic AAV injections into the NTS. C.L. and J.L. assisted with three-dimensional tissue clearing of brain and spleen samples. S.L. reanalyzed publicly available single-cell RNA-sequencing data. H.L. assisted with flow cytometric experiments and analysis. F.L. assisted with LCMV propagation and detection. W.L. is responsible for the management of

experimental animals. C.Z., N.X. and H.H. contributed to study supervision and data interpretation. K.M. and C.L. wrote the manuscript. K.M. supervised the project.

Competing interests

The authors declare no competing interests.

Methods references

64 Wu, J. *et al.* Cecal necroptosis triggers lethal cardiac dysfunction in TNF-induced severe SIRS. *Cell Reports* **43**, 114778 (2024). https://doi.org/10.1016/j.celrep.2024.114778

65 Zhang, Y. *et al.* A unique death pathway keeps RIPK1 D325A mutant mice in check at embryonic day 10.5. *PLoS Biol* **19**, e3001304 (2021). https://doi.org/10.1371/journal.pbio.3001304

66 Wu, Z. *et al.* The p75 neurotrophin receptor controls the skeletal stem cell niche through sensory innervation. *Developmental Cell* **61**, 259–275.e257 (2026). https://doi.org/10.1016/j.devcel.2025.09.012

67 Cao, K. *et al.* IL-33/ST2 plays a critical role in endothelial cell activation and microglia-mediated neuroinflammation modulation. *Journal of Neuroinflammation* **15**, 136 (2018). https://doi.org/10.1186/s12974-018-1169-6

68 Xu, L. *et al.* The transcription factor TCF-1 initiates the differentiation of TFH cells during acute viral infection. *Nature Immunology* **16**, 991–999 (2015). https://doi.org/10.1038/ni.3229

69 Ding, X. *et al.* Panicle-Shaped Sympathetic Architecture in the Spleen Parenchyma Modulates Antibacterial Innate Immunity. *Cell Reports* **27**, 3799–3807.e3793 (2019). https://doi.org/10.1016/j.celrep.2019.05.082

Supplementary Files

This is a list of supplementary files associated with this preprint. Click to download.

- SupplementaryvideoS2.mp4
- SupplementaryvideoS1.mp4